جامعة بيرزيت

BIRZEIT UNIVERSITY

SHAPE COEXISTENCE IN GERMANIUM AND SELENIUM ISOTOPES USING COVARIANT DENSITY FUNCTIONAL THEORY

التواجد الثنائي في نظائر الجرمانيوم والسلينيوم باستخدام نظرية كثافة الدالة

A thesis submitted in partial fulfillment
of the requirements for the Masters degree
in Physics

Nihad Jamal Abuawwad

Supervised by :
Dr. Hazem Abusara

BIRZEIT UNIVERSITY
Birzeit, Palestine

2018

SHAPE COEXISTENCE IN GERMANIUM AND SELENIUM ISOTOPES USING COVARIANT DENSITY FUNCTIONAL THEORY

التواجد الثنائي في نظائر الجرمانيوم والسلينيوم باستخدام نظرية كثافة الدالة

A thesis submitted in partial fulfillment
of the requirements for the Masters degree
in Physics

Nihad Jamal Abuawwad

Supervised by :
Dr. Hazem Abusara

BIRZEIT UNIVERSITY
Birzeit, Palestine

2018

SHAPE COEXISTENCE
IN GERMANIUM AND SELENIUM ISOTOPES

A thesis submitted in partial fulfillment
of the requirements for the Masters degree
in Physics

By:
Nihad Jamal Abuawwad

Thesis committee :
Dr. Hazem Abusara (Principle advisor)
Prof. Henry Jaqaman (Member)
Dr.Esmael Badran (Member)

This Thesis was submitted in partial fulfillment of the requirements for the Master Degree in Physics from the Factually Graduated Studies at Birzeit, Palestine

2018

Declaration

I, Nihad J. Abuawwad, declare that this thesis titled, 'SHAPE COEXISTENCE IN GERMANIUM AND SELENIUM ISOTOPES' and the work presented in it are my own

Dr. Hazem Abusara (Supervisor):

Prof. Henry Jaqaman (Committee Member) :

Dr. Esmael Badran (Committee Member) :

Dedication

To my father, "thank you" feel likes a really tiny word, but thank you from the deepest part of my heart for taking care of me throughout my life. My mother, grace for your soul. To my stepmother, I am sure you took care of me because you are an amazing, strong, and intelligent woman. To my sisters and brothers for their encouragement. To my amazing friend.

Acknowledgements

Firstly, I would like to express my sincere gratitude to my Thesis supervisor Dr. Hazem Abusara for his continues support and assistance from the first day until the final steps in this thesis. I would also like to thank members of my committee, Dr. Esmael Badran and Prof. Henry Jaqaman, for reviewing my thesis. I would like to thank to the amazing faculty who taught me the physics classes.

Abstract

Shape coexistence, shape evolution, and ground state properties such as; binding energy, two neutron separation energy, proton and neutron radii in the Ge and Se isotopic chains are studied within the frame work of relativistic-Hartree-Bogoliubov using density-dependent zero and finite range, and non-linear NN interactions.

A systematic investigation of the ground state shape is performed for Ge isotopes (Z = 32, $34 \leq N \leq 62$) and Se isotopes (Z = 34, $34 \leq N \leq 62$). The ground state shape is found to be both oblate and prolate ^{66}Ge and spherical and oblate for ^{72}Ge. The rest of the isotopic chain has only one minimum and in some ceases it is found to be triaxial. A sudden change in the nuclear shape is observed for ^{70,72,74}Ge isotopes.

For the Se isotopes the existing of two different shapes in the ground state is better seen as compared with Ge isotopes. It is clearly seen at the neutron rich side of the isotopic chain, and in the neutron deficient side of the chain one can see oblate-prolate and prolate-spherical shape transition. Our calculations is independent of the choice of parametrization, as we get similar results with both NL3*, and DD-PC1.

The physical properties: Binding energy, two neutron energy, neutron, proton, and charge radii are studied as a function of mass number or neutron number. In general a smooth change in these properties is found, except near $N = 50$ one can see a sharp change, which reflect the sudden change in the ground state deformation in the neighboring nuclei.

Our calculations shows a reasonable agreement with experimental data, and the results obtained with IBM based on Gogny density functional with D1M force.

ملخص

في هذه الدراسة سنقوم بدراسة التواجد الثنائي لأشكال الانوية وبعض الخصائص النووية كطاقة الربط، وطاقة فصل النيوترونات، ونصف قطر كلا من البروتون والنيوترون في مستوى الطاقة الأرضي لنظائر الجرمانيوم والسلينيوم باستخدام نظرية كثافة الدالة، بالاعتماد على الكثافة ذات المجال الصفري والنهائي، وبالاعتماد أيضا على التفاعلات غير الخطية للنيوكليونات.

وبناء على الحسابات التي قمنا بها لنظائر الجرمانيوم (العدد الذري =٣٢، وعدد النيوترونات من ٣٤ الى ٦٢) ونظائر السلينيوم (العدد الذري =٣٤، وعدد النيوترونات من ٣٤ الى ٦٢). قد تبين أن النواة في مستوى الطاقة الأرضي تأخذ الشكلين المفلح والمتضخم معا في نظير الجرمانيوم ٦٦، لكنها تأخذ الشكل الكروي والمفلطح في النظير ٧٢. وقد تبين أن هناك تغير فجائي في مستوى الطاقة الارضي في كل من نظائر الجرمانيوم (٧٠،٧٢،٧٤). التواجد الثنائي أكثر وضوحا في نظائر السلينيوم اذا ما قمنا بمقارنتها بنظائر الجرمانيوم.

جميع حساباتنا لا تعتمد على اختيار النموذج الذي نجري فيه هذه الحسابات سواء كان نموذج التفاعل غير الخطي أو نموذج التفاعل الكثافي الفعال. كما أن جميع حساباتنا تعطي قيم معقولة مقارنة بالقيم العملية والمحسوبة من تفاعل غوغني لكل من خصائص مستوى الطاقة الأرضي التي ذكرت سابقا.

Contents

List of Figures

List of Tables

Chapter 1
Introduction

In many mass regions through out the nuclear chart the nucleus in the ground state take different shapes at the same energy level, this phenomena is called shape coexistence[1–6]. Shape coexistence has become very important measure to explain the stability of the nucleus into a spherical shape, and the strong correlations (quadrupole) that characteristic the nucleus into a deformed shapes in around mid-shell regions. This region has become an important new testing ground for many types of nuclear structure models because of the richness of different collective motions and structures which are found in this region [7–9].

The shape coexistence can be studied experimentally and theoretically through different techniques and nuclear models such as complete spectroscopy and coulomb excitation, interacting bosons model (IBM), relativistic and non relativistic models using Hartree-Fock-Bogolibov (HFB) and self-consistent Hartree-Fock (HF) models [10–20].

The Coulomb excitation is a technique in experimental nuclear physics used to study the nuclear structure, where a nucleus is excited by an inelastic collision with

another nucleus through the electromagnetic interaction, and it allows measuring electromagnetic moments that related to the nuclear shape directly [21, 22]. If the electromagnetic moments has a positive value, then the shape is a prolate, and when it has a negative value, then the shape is an oblate. Spectroscopy and coulomb excitation have been used to probe shells and shape evolution far from stability for light nuclei [23]. They have been used to determine the energies of excited states of nuclei, their spins, and the probabilities of electromagnetic transitions. In addition, it has been possible to measure the electrical quadrupole moment of the nucleus by measuring the angular distribution of the gamma quanta in a magnetic field, also it used to measure the dipole magnetic moment of the excited nucleus [24–26].

In the interacting boson model (IBM) [27] the nucleons (protons or neutrons) pair up, essentially behaving like a single particle with boson properties. It was introduced in 1974 to describe collective properties of nuclei. Since 1974, the model has been used in many investigations and it has been extended to cover most nuclear structure, so it has can be used to predict vibrational and rotational modes of non - spherical nuclei [28, 29]. The basic assumption of interacting boson model that the nucleon pairs are represented by bosons with angular momenta L = 0 or 2. The pair with angular momentum 0 are called s-bosons, those with angular momentum 2 are called d-bosons [30, 31].

Nuclear structure models based on the mean field approximation have been successfully used to study the ground-state properties of nuclei all over the nuclear

chart. The mean field approximation based on non-relativistic and relativistic realization self - consistent Hartree-Fock (HF) and Hartree-Fock-Bogolibov (HFB) models, and the mean field approximation based on effective interaction, a zero-range skyrme force, finite range Gongy force [32, 33].

In the Hartree-Fock approach, the starting point is a Hamiltonian containing kinetic energy term, and potential term, and the wave function of the system can be written as a Slater determinant of one - particle spin - orbitals. Then the components of this Slater determinant (individual wave functions of the nucleons) are determined. To this end, it is assumed that the total wave function (the Slater determinant) is such that the energy is minimum [34, 35].

The relativistic Hartree-Fock-Bogolibov (RHFB) equations are solved by expanding the different components of the quasi-particle spinors in the complete set of eigne-solutions of the dirac equations with Woods-Saxon potentials [36]. In this model nucleons interact by exchange of virtual particles such as mesons. Then to solve the problem by this model, first, build the lagrangian containing these interaction terms. Second, gets a set of equations of motion. The nucleons obey the dirac equation, while the mesons obey the klein-Gordon equation [37].

All theses previous techniques and models was successfully applied to the study of shape evolution and shape coexistence. In 2007, J.Ljungvall, et al, investigated shape coexistence by Coloumb spectroscopy of ^{66}Se [38], and their results support a favored oblate ground-state deformation in ^{66}Se and ^{65}As. In 2002, Yosuke Toh studied the shape coexistence of Ge and Se with Complete Spectroscopy and

Coulomb Excitation, by calculating the means of multiple Coulomb excitation, and used it to determine the properties of the nuclear states [39].

Recently there have been studies on nuclear shape transitions and shape coexistence by IBM [40–43]. In 2014, J.E.Garcia-Ramos, K.Heyde, et al, studied the Shape evolution and shape coexistence in Po isotopes chain using interacting boson model with configuration mixing (IBM-CM) [44]. They obtained the IBM Hamiltonian and calculated excitation energies, B(E2)'s, electric quadrupole moments, nuclear radii and isotopic shifts, quadrupole shape invariants, wave functions, and deformations. Their results agrees with the experimental data for all the studied observables [45].

In 2017, K.Nomura, et al, studied the shape transitions and shape coexistence in the Ge and Se isotopes within the interacting boson model (IBM) with the microscopic input from a self-consistent mean-field calculation based on the Gogny - D1M energy density functional, They discuses the potential energy surface, the ground state properties, and the pairing energy for proton and neutron in Ge and Se isotopes. The Gogny - D1M energy surfaces predict the coexistence between the prolate and oblate shapes in the lightest nuclei in both isotopic chains. For shapes around N = 40 coexistence between spherical and γ-soft (i.e. the energy does not change with the value of gamma) shapes is observed, When neutron number increases towards the N = 50 shell closure weakly deformed prolate shapes are obtained. On the other hand, for $52 \leqslant N \leqslant 62$ a number of nuclei exhibiting γ-soft shapes *(which means the nucleus shape changed smoothly in isotopes chain)* and coexistence between prolate and oblate shapes are observed [46]. He also studied

the shape evolution in Kr isotopes using the same models but with input coming from a self-consistent mean-field calculation based on the Gogny energy density functional and relativistic HFB with DD-PC1 and DD-ME2 parameterizations. For neutron deficient isotopes there is no notable difference between both relativistic and collectivistic models. However, they provide different prediction for neutron rich isotopes[47].

In 2007, Lu Guo, et al study the ground-state deformations of the Ge isotopes in Hartree-Fock-Bogoliubov (HFB) used Gogny force. The deformations and binding energies are calculated with good agreement with experimental data, also the Ge isotopes take a triaxial shapes in most cases [48].

Also in 1997, S. K. Patra, et al, study the structural Properties of Ne, Mg, Si, S, Ar and Ca Nuclei by relativistic mean field theory using three sets of force parameter, the NL2, NL-SH and TM2. The ground state shapes (prolate, oblate or spherical) are investigated for these nuclei, also the deformations of nuclei near the magic shell N=28 are found to be large. Finally, A large number of cases of shape coexistence are identified [49]. Moreover, in 2002, T. Niksic, et al investigate axially the ground state shape in Hg and Pb nuclei in this model framework used NL3* effective interaction, and the behave of shape with increasing neutron number exchange from spherical into an oblate minimum, and a pronounced minimum develops on the prolate in Hg isotopes, also in Pb isotopes with increasing neutron number, however, the oblate minimum is lowered in energy and the nuclei $^{188-194}Pb$ have oblate ground states [50].

In 2017, H Abusara, et al, investigated the shape within relativistic Hartree-Fock-Bogoliubov (HFB) based on density - dependent zero and finite range NN interactions for Kr (Z= 36,34 $\leqslant N \leqslant$ 64), Sr(Z=38, 34 $\leqslant N \leqslant$ 64) and Zr (Z= 40, 48 $\leqslant N \leqslant$ 70) isotopes [51]. The shape of ground state is smooth in Kr isotopes while it is not smooth in Sr isotopes, and this is reflected on the physical prosperities of ground state such as binding energy, proton, neutron, charge radius in these isotopes.

In 2017, H Abusara, et al, studied the shape coexistence and triaxiality softness in Mo (Z= 42,52 $\leqslant N \leqslant$ 68), and Ru (Z= 44,52 $\leqslant N \leqslant$ 68) isotopes within Relativistic-Hartree-Bogoliubov (RHB) based on DD-ME2 and DD-PC1 parameterizations. Shape coexistence does not show up in Ru isotopes except in ^{104}Ru, on the other hand shape coexistence is a clear in Mo isotopes. Moreover, triaxiality softness is clear in both chain isotopes [2].

In the present analysis, we will perform a systematic calculation to investigate the shape coexistence in Ge and Se isotopes using the relativistic - Hartree - Bogoliubov (RHB) using NL3*, DD-ME2, and DD-PC1 forces, and we will discuses the binding, separation energies for neutrons. Then we will discuss the results and compared it with other models such as interacting bosons model, and non-relativistic Hartree - Bogoliubov based on Gogny-D1S [52].

This thesis is organized as follows: in CHAPTER 2 contains the formalism of the model in the RHB formalism. In CHAPTER 3 and CHAPTER 4 potential energy surfces and physical properties for the ground state for Ge and Se isotopes

are presented, respectively. In CHAPTER 5 summary and main result will be presented.

Chapter 2

Formalism

2.1 Covariant Density Functional Theory

The Density functional is a tool for a microscopic description of nuclei. It is successful in determining properties of nuclear ground states such as binding energies, radii, or deformation parameters [53, 54]. Three type of models have been developed to provide a relativistic density functional, the nonlinear meson nucleon coupling model, the density-dependent meson nucleon coupling model, and a density-dependent point coupling model. The main difference between them is the treatment of the range of the interaction, the mesons, and density dependence. The interaction in the first two classes has a finite range, while the third class uses zero-range interaction [55–58].

2.2 Lagrangian density

2.2.1 Lagrangian density in general

A classical relativistic field theory starts from a number of fields $q_j(x)$. Their dynamics is determined through a Lagrangian density $\mathcal{L}(q, \partial_\mu q, t)$ and the variational principle

Starting from classical Lagrangian density

$$\delta \int \partial^4 x \mathcal{L}(q, \partial_\mu q, t) = 0 \tag{2.1}$$

$$\partial_\mu (\frac{\partial L}{\partial(\partial_\mu q_j)}) - (\frac{\partial L}{\partial q_j}) = 0 \tag{2.2}$$

from the following Lagrangian density

$$\mathcal{L} = \mathcal{L}_{Nucleon} + \mathcal{L}_{Meson} + \mathcal{L}_{int} \tag{2.3}$$

It contains free nucleons described by the Lagrangian density

$$\mathcal{L}_{Nucleon} = \bar{\psi} \left(i\gamma_\mu \cdot \partial_\mu - m \right) \psi \tag{2.4}$$

where is m the mass of nucleons, and ψ is the Dirac spinor, so the Lagrangian density for σ meson

$$\mathcal{L}_\sigma = \frac{1}{2}(\partial_\mu \sigma \partial^\mu \sigma - m_\sigma^2 \sigma^2) \tag{2.5}$$

The Lagrangian for π mesons

$$\mathcal{L}_\pi = \frac{1}{2}(\partial_\mu \pi \partial^\mu \pi - m_\pi^2 \pi^2) \tag{2.6}$$

The Lagrangian for ω mesons

$$\mathcal{L}_\omega = -\frac{1}{2}(\frac{1}{2}\Omega_{\mu\nu}\Omega^{\mu\nu} - m_\omega^2 \omega_\mu \omega^\mu) \tag{2.7}$$

The Lagrangian for ρ mesons

$$\mathcal{L}_\rho = -\frac{1}{2}(\frac{1}{2}\vec{R}_{\mu\nu}\vec{R}^{\mu\nu} - m_\rho^2 \rho_\mu \rho^\mu) \tag{2.8}$$

The Lagrangian for *photon*

$$\mathcal{L}_\mathcal{A} = -\frac{1}{4}(\vec{F}_{\mu\nu}\vec{F}^{\mu\nu}) \tag{2.9}$$

Where the $\Omega_{\mu\nu}$, $\vec{R}_{\mu\nu}$, and $\vec{F}_{\mu\nu}$ are the field tensors given by this is equations :

$$\omega_{\mu\nu} = \partial_\mu \Omega_\nu - \partial_\nu \omega_\mu \tag{2.10}$$

$$\vec{\mathcal{R}}_{\mu\nu} = \partial_\mu \rho_\nu - \partial_\nu \rho_\mu \tag{2.11}$$

$$\vec{\mathcal{F}}_{\mu\nu} = \partial_\mu A_\nu - \partial_\nu A_\mu \tag{2.12}$$

The interaction between the nucleons and the mesons described by given Lagrangian

$$\mathcal{L}_{int} = -g_\sigma \bar{\psi}\psi\sigma - g_\omega \bar{\psi}\gamma_\mu\psi\omega_\mu - g_\rho \bar{\psi}\gamma_\mu\vec{\tau}\psi\vec{\rho}_\mu - e\bar{\psi}\gamma_\mu(\frac{1-\tau_3}{2})\psi A_\mu \tag{2.13}$$

2.2.2 The meson-exchange model

In the meson exchange model the nucleus is described as a system of point like nucleons, Dirac spinors, coupled to mesons and to the photons. The nucleons interact by the exchange of several mesons, namely a scalar meson s and three vector particles,σ, ω, ρ, and the photon [59, 60]. These mesons are defined by three quantum numbers; spin (J), parity (P) and isospin(T). Mesons that participate in this interaction are [61] :

1. The isoscalar scalar σ meson, has quantum numbers (J = 0, T = 0 and P = 1),and the corresponding field is a scalar field produce attraction.

2. The isoscalar vector ω, has quantum numbers (J=1, T=0, P=-1), and the corresponding field is a vector field produce the repulsion.

3. The isovector vector ρ- meson, has quantum numbers (J=1,T=1, P=-1), and it couple to the iso vector current.

Starting on a more fundamental level, one therefore introduces a relativistic Lagrangian describing point-like nucleons interacting through the exchange of different types of mesons.

$$\begin{aligned}\mathcal{L} = \bar{\psi}\left(\gamma(i\partial_\mu - g_\omega\omega - g_\rho\vec{\rho}\vec{\tau} - eA) - m - g_\sigma\sigma\right)\psi \\ +\frac{1}{2}(\partial\sigma)^2 - \frac{1}{2}m_\sigma^2\sigma^2 - \frac{1}{4}\Omega_{\mu\nu}\Omega^{\mu\nu} + \frac{1}{2}m_\omega^2\omega^2 \\ -\frac{1}{4}\vec{R}_{\mu\nu}\vec{R}^{\mu\nu} + \frac{1}{2}m_\rho^2\vec{\rho}^2 - \frac{1}{4}F_{\mu\nu}F^{\mu\nu}\end{aligned} \tag{2.14}$$

where ψ is the Dirac spinors described the nucleons, m the mass of mesons, and g the coupling constant.

To treat the density dependence in this model Boguta and Bodmer replacing the mass term by a quadratic a-potential of the form:

$$U(\sigma) = \frac{1}{2}m_\sigma^2\sigma^2 + \frac{1}{3}g_2\sigma^3 + \frac{1}{4}g_3\sigma^4 \tag{2.15}$$

and the ω mesons, replacing the mass term by a quadratic a potential of the form :

$$U(\omega_\mu) = \frac{1}{2}m_\omega^2\omega^\mu\omega_\mu + \frac{1}{4}c_3(\omega^\mu\omega_\mu) \tag{2.16}$$

and the ρ mesons, replacing the mass term by a quadratic a potential of the form :

$$U(\vec{\rho}_\mu) = \frac{1}{2}m_\rho^2\vec{\rho}^\mu\vec{\rho}_\mu + \frac{1}{4}c_3(\vec{\rho}^\mu\vec{\rho}_\mu) \tag{2.17}$$

The Lagrangian (2.14) contains as parameters the meson masses m_σ, m_ω, and m_ρ and the coupling constants g_σ, g_ω, and g_ρ, and e is the charge of the protons and it vanishes for neutrons.

The density-dependent meson-nucleon coupling model has an explicit density dependence for the meson-nucleon vertices. The coupling constant dependence is defined as:

$$g_i(\rho) = g_i(\rho_{sat})f_i(x) \tag{2.18}$$

i can be any of the three mesons σ,ω, and ρ where the density dependence is given by

$$f_i(x) = a_i\frac{1 + b_i(x + d_i)^2}{1 + c_i(x + d_i)^2}. \tag{2.19}$$

for σ and ω and by

$$f_\rho(x) = \exp(-a_\rho(x - 1)). \tag{2.20}$$

for the ρ meson.

x is defined as the ratio between the baryonic density ρ at a specific location and the baryonic density at saturation ρ_{sat} in symmetric nuclear matter. The eight parameters are not independent, but constrained as follows: $f_i(1) = 1$, $f''_\sigma(1) = f''_\omega(1)$, and $f''_i(0) = 0$. These constrains reduce the number of independent parameters for density dependence to three. In our study this model is represented by the parameter set NL3*, and DD-ME2 given in tables 2.1, and 2.2.

TABLE 2.1: NL3* parameterization in RMF Lagrangian

parameter	NL3$*$
m	939
m_σ	502.5742
g_σ	10.0944
a_σ	0.00000
b_σ	0.00000
c_σ	0.00000
d_σ	0.00000
m_ω	782.600
g_ω	12.8065
a_ω	0.00000
b_ω	0.00000
c_ω	0.00000
d_ω	0.00000
m_ρ	763.000
g_ρ	4.5748
a_ρ	0.00000

TABLE 2.2: DD-ME2 parameterization in RMF Lagrangian

parameter	DD-ME2
m	939
m_σ	550.1238
g_σ	10.5396
a_σ	1.3881
b_σ	1.0943
c_σ	1.7057
d_σ	0.4421
m_ω	783.000
g_ω	13.0189
a_ω	1.3881
b_ω	0.9240
c_ω	1.4620
d_ω	0.4775
m_ρ	763.000
g_ρ	3.6836
a_ρ	0.5647

2.2.3 The point-coupling model

The point-coupling model is another way to construct a relativistic density function. In this model the mesons exchange replaced by interaction between the nucleons. Nonlinear point-coupling models have been applied successfully to describe infinite nuclear matter [64, 65].

The Lagrangian for the density point coupling model is given by :

$$\begin{aligned}\mathcal{L} &= \bar{\psi}\left(i\gamma_\mu \cdot \partial_\mu - m\right)\psi - \frac{1}{2}\alpha_S(\hat{\rho})\left(\bar{\psi}\psi\right)\left(\bar{\psi}\psi\right) - \frac{1}{2}\alpha_V(\hat{\rho})\left(\bar{\psi}\gamma^\mu\psi\right)\left(\bar{\psi}\gamma_\mu\psi\right) \\ &- \frac{1}{2}\alpha_T V(\hat{\rho})\left(\bar{\psi}\vec{\tau}\gamma^\mu\psi\right)\left(\bar{\psi}\vec{\tau}\gamma_\mu\psi\right) - \frac{1}{2}\delta_S\left(\partial_v\bar{\psi}\right)\left(\partial^v\bar{\psi}\right) \\ &- e\bar{\psi}\gamma \cdot A\frac{(1-\tau_3)}{2}\psi \qquad (2.21)\end{aligned}$$

TABLE 2.3: DD-PC1 parameterizations in RMF Lagrangian

parameter	DD-PC1
m	939
a_σ	-10.04616
b_σ	-9.15042
c_σ	-6.42729
d_σ	1.37235
a_ω	5.91946
b_ω	8.86370
d_ω	0.65835
b_ρ	1.83595
d_ρ	0.64025

It contains the free-nucleon Lagrangian, the point-coupling interaction terms. The derivative terms accounts for the leading effects of finite-range interaction [66]. This model contains isosclar-scalar, isoscalar-vector, and isovector-vector. It is represented by the DD-PC1 as has been seen in table(2.3).

2.3 The Hamiltonian and the equation of motion

From the Lagrangian density in Eq.(2.14), the Hamiltonian operator is :

$$\mathcal{H} = \int \partial^3 r(\sum_m P_m - \partial_t \phi_m - \mathcal{L}(r)) \tag{2.22}$$

where : $\phi_m = (\psi,\, \sigma,\, \omega_\mu,\, \vec{\rho_\mu},\, A_\mu)$ P_m is the momentum conjugate operator

$$\mathcal{P}_m = \frac{\partial \mathcal{L}}{\partial(\partial\phi_m/\partial t)} \tag{2.23}$$

The Hamiltonian density of the nucleon - mesons interacting is

$$\mathcal{H} = \mathcal{H}_\psi + \mathcal{H}_\sigma + \mathcal{H}_\omega + \mathcal{H}_\rho + \mathcal{H}_A + \mathcal{H}_{int} \tag{2.24}$$

where:

$$\mathcal{H}_\psi = \bar{\psi}(\alpha \cdot p + \beta m)\psi \tag{2.25}$$

$$\mathcal{H}_\sigma = -\frac{1}{2}\sigma\Delta\sigma + U_\sigma(\sigma) \tag{2.26}$$

$$\mathcal{H}_\omega = \frac{1}{2}\omega_\mu\omega^\mu - U_\omega(\omega) \tag{2.27}$$

$$\mathcal{H}_\rho = \frac{1}{2}\vec{\rho_\mu}\Delta\vec{\rho^\mu} - U_\rho(\rho) \tag{2.28}$$

$$\mathcal{H}_A = \frac{1}{2}A_\mu A^\mu \tag{2.29}$$

$$\mathcal{H}_{ins} = (g_\sigma\sigma\bar{\psi}\psi + g_\omega\omega_\mu\bar{\psi}\gamma^\mu\psi + g_\rho\vec{\rho_\mu}\bar{\psi}\gamma^\mu\vec{\tau}\psi + e(\frac{1-\tau_3}{2})A_\mu\bar{\psi}\gamma^\mu\psi) \tag{2.30}$$

In the Haretree method, the stationary Dirac equation for the nucleons is :

$$\hat{h}_D \psi_i = \epsilon_i \psi_i \tag{2.31}$$

where h_D is the Hamiltonian of the nucleons with mass m

$$\hat{h}_D = \alpha(-i\nabla - V(r)) + V_0(r) + \beta(m + S(r)) \tag{2.32}$$

the Hamiltonian contains the attractive scalar field S(r)

$$S(r) = g_\sigma \sigma(r) \tag{2.33}$$

and the repulsive time like component of the vector $V_0(r)$

$$V_0(r) = g_\omega \omega_0(r) + g_\rho \tau_3 \rho_0(r) + e\frac{1-\tau_3}{2} A_0(r) \tag{2.34}$$

and the magnetic potential V(r)

$$V(r) = g_\omega \omega(r) + g_\rho \tau_3 \rho(r) + e\frac{1-\tau_3}{2} A(r) \tag{2.35}$$

Note that in these eqnarray, the four-vector components of the vector field $(\omega^\mu, \rho^\mu, A^\mu)$ are separated into the time-like (ω_0, ρ_0, A_0) and the space-like components $[\omega = (\omega^x, \omega^y, \omega^z), \rho = (\rho^x, \rho^y, \rho^z), A = (A^x, A^y, A^z)$].

The corresponding mesons Fields and the electromagnetic field are determined by the Klein-Gordon equations:

$$(-\nabla^2 + m_\sigma^2)\sigma(r) = -g_\sigma \rho_s(r) - g_2\sigma^2(r) - g_3\sigma^3(r) \tag{2.36}$$

$$(-\nabla^2 + m_\omega^2)\omega_0(r) = g_\omega \rho_\nu \tag{2.37}$$

$$(-\nabla^2 + m_\omega^2)\omega_\mu(r) = g_\omega j_\mu \tag{2.38}$$

$$(-\nabla^2 + m_\rho^2)\rho_0(r) = g_\omega \rho_3 \tag{2.39}$$

$$(-\nabla^2 + m_\rho^2)\vec{\rho}_\mu(r) = g_\rho \vec{j}_\mu \tag{2.40}$$

$$-\nabla^2 A_0(r) = e\rho_p(r) \tag{2.41}$$

$$-\nabla^2 A_\mu(r) = e\rho_\mu^p(r) \tag{2.42}$$

with source terms involving the various nucleonic densities and currents

$$\rho_s(r) = \sum_{i=1}^{N} \bar{\psi}_i(r)\psi_i(r) \tag{2.43}$$

$$\rho_\nu(r) = \sum_{i=1}^{A} \psi_i^+(r)\psi_i(r) \tag{2.44}$$

$$\rho_3(r) = \sum_{i=1}^{A} \psi_i^+(r)\tau_3\psi_i(r) \tag{2.45}$$

$$\rho_p(r) = \sum_{i=1}^{A} \psi_i^+(r)(\frac{1-\tau_3}{2})\psi_i(r) \tag{2.46}$$

$$j_\mu(r) = \sum_{i=1}^{A} \bar{\psi}_i(r)\gamma_\mu\psi_i(r) \tag{2.47}$$

$$\vec{j}_\mu(r) = \sum_{i=1}^{A} \bar{\psi}_i(r)\gamma_\mu\vec{\tau}\psi_i(r) \tag{2.48}$$

In the ground-state solution for an even-even nucleus spatial vector A(r) is neglected in the calculations, because the coupling constant of the electromagnetic interaction is small compered with the coupling constant of the mesons, and there are no currents (time-reversal invariance) [56].

The components of the vector ω and ρ mesons lead to the interactions between possible currents. For the ω meson the interaction is attractive for all combinations (pp, nn, pn), and for ρ mesons it is attractive for pp and nn currents but repulsive for pn currents [57]. The shape coexistence in CDFT framework depends on the

spatial components of ω meson, so there are only two parameters (the mass m_ω and the coupling constant g_ω) of the ω meson define the properties of the shape coexistence [Eqs.(2.35, 2.38, 2.40)].

The solution of the CDFT equations corresponds to the ground state of the nucleus it is corresponding to a local minimum in the potential energy surface, so to obtain the solution for any point we used the constrained of quadrupole mass moment. The constrained calculations are performed by imposing constraints on both axial and triaxial mass quadrupole moments [2]. The method of quadratic constraints uses an unrestricted variation of the function

$$\langle \hat{H} \rangle + \sum_{\mu=0,2} C_{2\mu} (\langle \hat{Q}_{2\mu} \rangle - q_{2\mu})^2 \tag{2.49}$$

where $\langle \hat{H} \rangle$ is the total energy, ($\langle \hat{Q_{2\mu}} \rangle$ denotes the expectation values of mass quadrupole operators,

$$\hat{Q}_{20} = 2z^2 - x^2 - y^2 \quad \text{and} \quad \hat{Q}_{22} = x^2 - y^2 \tag{2.50}$$

where: $q_{2\mu}$ is the constrained value of the multipole moment.

$C_{2\mu}$ is the corresponding stiffness constant.

$\sum_{\mu=0,2} \lambda_\mu \hat{Q}_{2\mu}$ is the quadratic constraint adds an extra force term to the system

where$\lambda_\mu = 2C_{2\mu}(\langle \hat{Q}_{2\mu} \rangle - q_{2\mu})^2$

This term is necessary for self consistent solution to force the system to a point in deformation space different from a stationary point. [2]

2.4 Pairing correlations

The BCS theory which can accommodate the pairing correlations in the ground states of atomic nuclei are presented [67, 68]. In mean field theory, The relativistic Hartree-Fock-Bogolibov model provides a description to particle-particle (pp) correlation used by pairing field potential $\hat{\Delta}$, and particle-hole (ph) correlation by self consistent field potential.

We take $|\phi>$ is the Slater determinate that represents the vacuum with quasi-particle [69], and the α_k, α_k^+ is the single-nucleons creation and annihilation operator which:

$$\alpha_k = \sum_n U_{nk} C_n^+ + V_{nk} C_n \tag{2.51}$$

where n is the index refers to original basis, and U,V are the Hartree - Bogoluibove wave function determined by variational method.

In the presence of pairing the single-particle density matrix is generalized to two densities: the normal density $\hat{\rho}$ and parity tensor $\hat{K}$

$$\rho_{nn'} =< \phi | C_n^+ C_n | \phi > \tag{2.52}$$

$$\mathcal{K}_{nn'} =< \phi | C_n C_n | \phi > \tag{2.53}$$

The total density functional is :

$$E_{RHB} = E_{RMF}[\rho] + E_{pair}[k] \tag{2.54}$$

where

$$E_{RHB}[\psi, \bar{\psi}, \sigma, \omega^{\mu}, \vec{\rho^{\mu}}, A^{\mu}] = \int d^3 r H(r) \tag{2.55}$$

$$E_{RMF} = \sum_{i=1}^{A} \int d^3 r \psi_i^{+}(\alpha p + \beta m) - \frac{1}{2}(\nabla A)^2 +$$

$$\frac{1}{2} e \int d^3 r j_p^{\mu} A_{\mu} + \frac{1}{2} \int d^3 r [\alpha_s \rho_s^2 + \alpha_{\nu} j_{\mu} j^{\mu} + \alpha_{TV} \vec{j_{\mu}} \cdot \vec{j^{\mu}} + \delta \rho_s \rho_s] \tag{2.56}$$

and the $E_{pair}[k]$ is

$$E_{pair}[k] = \frac{1}{4} \sum_{n_1 n_1{}'} \sum_{n_2 n_2{}'} K_{n_1 n_1'} < n_1 n_1{}' | V^{PP} | n_2 n_2{}' > K_{n_2 n_2{}'} \tag{2.57}$$

where $< n_1 n_1^{'} | V^{PP} | n_2 n_2^{'} >$ is the matrix element of the two body interaction.

$$V^{pp}(r_1, r_2, r_1^{'}, r_2^{'}) = -G\delta(R - R^{'}) P(r) P(r^{'}) \tag{2.58}$$

$$R = \frac{1}{\sqrt{2}}(r_1 + r_2) \tag{2.59}$$

$$r = \frac{1}{\sqrt{2}}(r_1 - r_2) \tag{2.60}$$

$$P(r) = (\frac{1}{4\pi a^2})^{3/2} \exp \frac{-r^2}{2a^2} \tag{2.61}$$

The RHB-coefficients U and V are obtained by the variational :

$$\begin{bmatrix} h_D - m - \lambda & \Delta \\ -\Delta^* & -h_D + m + \lambda \end{bmatrix} \begin{bmatrix} U_K \\ V_K \end{bmatrix} = E_K \begin{bmatrix} U_K \\ V_K \end{bmatrix} \tag{2.62}$$

In (RMFT) the single nucleons has Dirac Hamiltonian h_D is a given in Eq.(2.31), λ is the chemical potential, m is the mass of nucleons, and Δ is the pairing field which is :

$$\Delta_{n_1 n_1'} = \frac{1}{2} \sum_{n_2 n_2'} < n_1 n_1' | V^{PP} | n_2 n_2' > K_{n_2 n_2'} \tag{2.63}$$

and

$$\begin{bmatrix} U_K \\ V_K \end{bmatrix} \tag{2.64}$$

it is an eignvector.

2.5 Nuclear shape and deformation

The deformation of the ground state(the nuclear shape), is one of the most fundamental properties of an atomic nucleus, along with its mass and radius. A

nucleus may take different shapes varying from spherical to quadrupole (prolate, oblate), and higher order multipole deformations [70].

The instantaneous coordinate R(t) of a point on the nuclear surface at (θ, ϕ) in terms of the spherical harmonics :

$$\mathcal{R}(\theta,\phi) = R_{avg}[1 + \sum_{\lambda} \sum_{\mu=-\lambda}^{\lambda} \alpha_{\lambda\mu} Y_{\lambda\mu}(\theta,\phi)] \tag{2.65}$$

In the first case when ($\lambda = 0$), that gives the monopole, and $\lambda = 1$, it is give the dipole deformation, but the important point for our study is when ($\lambda = 2$), which give the quadrupole deformation. For a quadruple-deformed nucleus with elliptical shape we can distinguish a coordinate frame defined by the three axes of deformation. For example we can define the long axis as z, the short axis as x and the intermediate axis as y (other choices are allowed as well). In this case we have five parameters $\alpha_{\lambda\mu}$, and this five parameters can be reduced to two real parameters α_{20}, α_{22}. We defined Hill-Wheeler coordinate in terms of α_{20} and α_{22}

$$\alpha_{20} = \beta \cdot \cos\gamma \tag{2.66}$$

$$\alpha_{22} = \frac{1}{\sqrt{2}}\beta \cdot \sin\gamma \tag{2.67}$$

We can connect the quadrupole constraint (2.50) with β, γ

$$\beta = \sqrt{\frac{4\pi}{5}}\frac{Q}{r^2} \tag{2.68}$$

where

$$Q = \sqrt{Q_{20}^2 + Q_{22}^2} \tag{2.69}$$

$$\gamma = tan^{-1}(\frac{Q_{22}}{Q_{20}}) \tag{2.70}$$

If we substitute Eqs .2.66,2.67 in Eq .2.65, then we obtain :

$$\mathcal{R}(\theta, \phi) = R_{avg}[1 + \beta\sqrt{\frac{5}{16\pi}}(\cos\gamma(3\cos^2\theta - 1) + \sqrt{3}\sin\gamma\sin^2\theta\cos 2\phi)] \tag{2.71}$$

Then we can calculate the increments of the three semi-axes as a function of β and γ

$$R_x = R(\frac{\pi}{2}, 0) = R_{avg} \cdot [1 + \beta \cdot \sqrt{\frac{5}{4\pi}} \cdot \cos(\gamma - \frac{2\pi}{3})] \tag{2.72}$$

$$R_y = R(\frac{\pi}{2}, \frac{\pi}{2}) = R_{avg} \cdot [1 + \beta \cdot \sqrt{\frac{5}{4\pi}} \cdot \cos(\gamma + \frac{2\pi}{3})] \tag{2.73}$$

$$R_z = R(0, 0) = R_{avg} \cdot [1 + \beta \cdot \sqrt{\frac{5}{4\pi}} \cdot \cos(\gamma)] \tag{2.74}$$

The shape can have axial symmetry, that in the nucleus have an ellipsoid shape and elongated along one of the axis. If it elongated along z-axis it will be prolate axial, and the perpendicular cross section is circular. In the case where the perpendicular cross section is not circular, then the shape of nucleus will be triaxial[71, 72]. In general if γ is a multiple of 60° then the shape is axial, and when γ is not a multiple of 60 it will be triaxial. Thus when γ is a multiple of 60° then the radius along two of the three axis in Eqs. 2.72, 2.73, 2.74 are equal. As we can see :

If $\gamma = 0$, the symmetry axis is Z axis, and $R_x = R_y$.

If $\gamma = 60$, the symmetry axis is Y axis, and $R_x = R_z$.

If $\gamma = 120$, the symmetry axis is X axis, and $R_y = R_z$.

Chapter 3

Ge isotopes

In this chapter we will calculate the axial potential energy curves (PEC), triaxial potential energy surfaces (PES), and from their results we will locate the deformation of the ground state. Physical properties as a function of neutron number for even - even Ge (Z = 32, $34 \leq N \leq 62$) isotopes will be studied. The axial calculations are performed using NL3*, DD-ME2, and DD-PC1 parameterizations, while the triaxial calculations are performed using NL3*, and DD-PC1 parameterizations.

3.1 Potential energy surface

In this section we perform constrained calculations on β (Eq. 2.68) and γ (Eq.2.70). If γ is constrained to 0° we obtain the axial potential energy curves. If the value of γ is varied between 0° and 60° for each value of β then we will obtain

the potential energy surfers as a function of both β and γ which will allow us to determine if there is a triaxial ground state minimum. Our results are compared with those obtained from relativistic Hartree-Fock-Bogolibouve within Gogny - D1S [52], and interacting bosons model (IBM) based on Gogny - D1M [46].

3.1.1 Axial symmetry

The ground state of Ge isotopes are confirmed to be oblate and prolate by experimental data on energy spectra and charge radii [73], but spherical low -lying minima are observed for N $<$ 110.

Figs.3.1, and 3.2 show the calculated potential energy curves for Ge(Z =32, 34 $\leq N \leq$ 62) isotopes. From these figures, one can see that these isotopes can be classified into three categories according to their ground state deformation. The first category contains isotopes that has only one minimum, namely ^{70,76,80,82}Ge. ^{70}Ge has an oblate minimum at $\beta = 0.2$, but ^{76,80}Ge have a prolate minimum at $\beta = 0.2$. On other hand ^{82}Ge has only spherical shape($\beta = 0$).

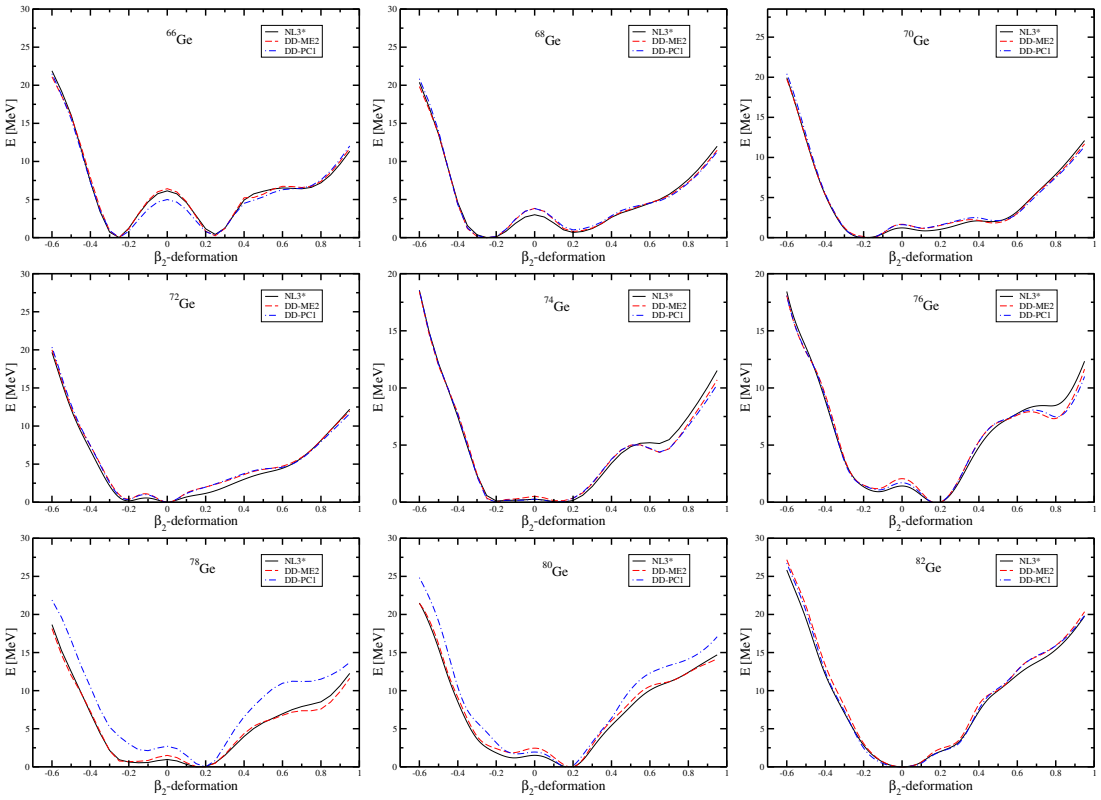

FIGURE 3.1: Potential energy curves of even-even Ge isotopes for neutron number $34 \leq N \leq 50$ as functions of the quadrupole deformation, obtained from an axial RHB calculations with constrained quadrupole deformation. The effective interactions used are NL3*, DD-ME2, and DD-PC1. The curves are scaled such that the ground state has a zero MeV energy

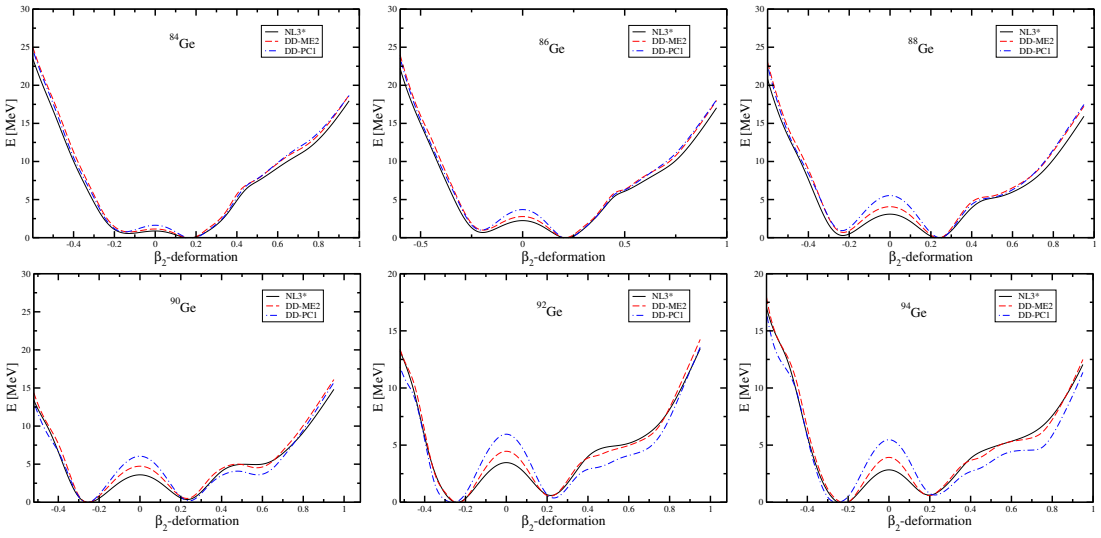

FIGURE 3.2: Similar to Fig. 3.1 but for neutron number $52 \leq N \leq 62$

The second category contains isotopes that has two minima, namely ^{66,68,84,86,90,92,94}Ge. In ^{66,90}Ge the ground state has two shapes (prolate and oblate) located at $|\beta| = 0.25$. Is similarly in ^{68}Ge there are two minima, the first minimum is a prolate located at $\beta = 0.25$, and the second minimum is an oblate at $\beta = 0.2$. However, the prolate minimum is less pronounced. Also^{84}Ge has a prolate, and oblate minima at $|\beta| = 0.15$, but in ^{86,88}Ge the prolate and oblate minima becomes more pronounced with $|\beta| = 0.2$. In ^{92,94}Ge exhibits coexisting prolate with minimum at $\beta = 0.2$, and oblate at $\beta = 0.25$.

The third category contains isotopes that has a flat minima, that is mean *the energy does not vary with β_2 in a ceratin region of PEC such as ^{74}Ge.* Finally, in some nuclei there is a one minimum behind the flat minima such as in ^{72,78}Ge, and this minima could be a prolate or oblate.

In Fig. 3.3 we show the ground state deformation for all categories extracted from Figs.3.1, and 3.2, and for D1S in taken from ref. [52]. For a prolate and oblate minima, the results are almost in full agreement with small deviation in the location of their minima. However, there is a a disagreement between our results in the D1S ref. [52] results, that is we only predict a prolate minimum for ^{76,78,80}Ge, while they predict an oblate one too.

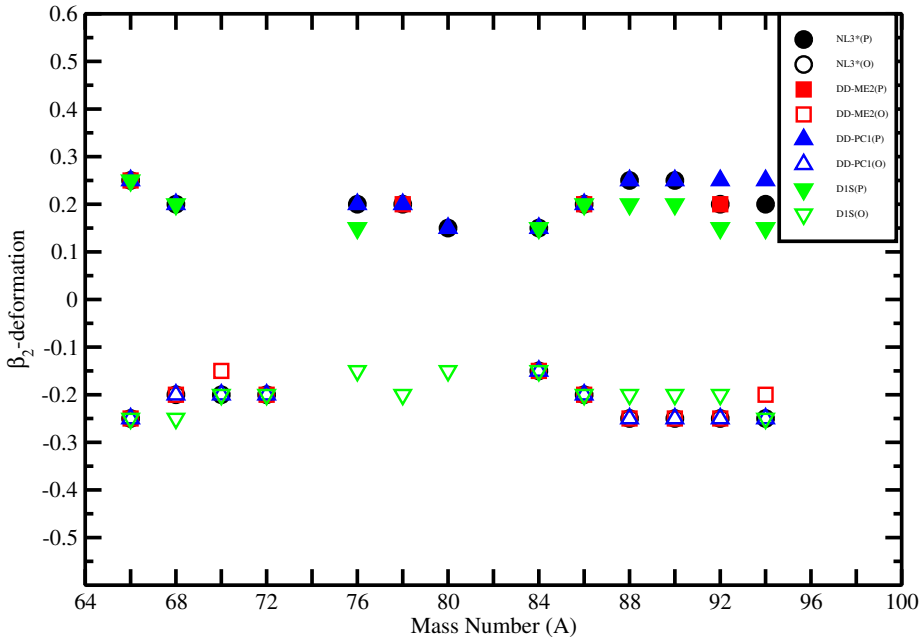

FIGURE 3.3: Quadrupole deformation parameters β_{20} for even-even Ge isotopes using NL3* (Circles), DD-ME2 (Squares), DD-PC1 (Up triangle) , and D1S [52] (Down triangle) as a function of mass number (A), Filled for a prolate, empty for an oblate, and no points for spherical shape

3.1.2 Triaxial symmetry

We perform constrained calculations on Q_{20}, Q_{22} using NL3*, and DD-PC1 parameterizations. Potential energy surfaces (PES) are shown in Fig 3.4. In Fig. 3.4 one can see that ^{66}Ge has two minima at $\beta = 0.25$, one of them is an oblate, and the other is a triaxial with $\gamma = 45$. The oblate minimum is the global. The shape of ground state in ^{68}Ge and ^{70}Ge becomes almost a triaxial at $\gamma = 55$ and an oblate at $\gamma = 60$, respectively, and both of them nuclei has only one minimum as we move along the isotopic chain into ^{72}Ge we will have two minima (spherical, and oblate at $\beta = 0.2$) with energy different 0.18 MeV, and the deepest one is the spherical minima. One can see that there is a sudden change in the ground

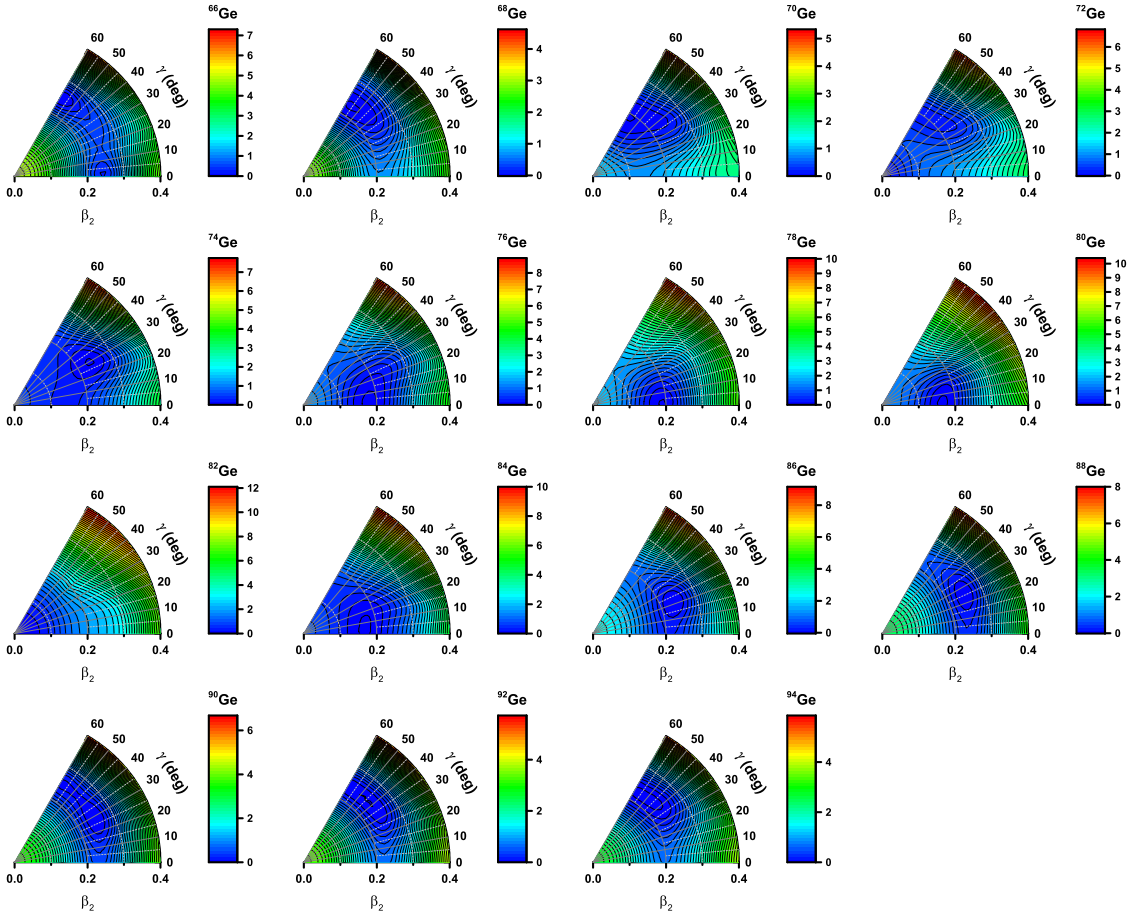

FIGURE 3.4: Potential energy surfaces of even-even Ge isotopes from neutron number ($34 \leq N \leq 62$) as functions of the quadrupole deformation, obtained from an triaxial RHB calculations with constrained quadrupole deformation. The effective interactions used are NL3*. The surfaces are scaled such that the ground state has a zero MeV energy

state deformation. In ^{74}Ge the minimum is a triaxial at $\beta = 0.25$, and $\gamma = 30$. For ^{76,78,80,84}Ge the global minimum is a prolate and the value of β_2 is decreasing from 0.2 to 0.15 leading to a spherical shape for ^{82}Ge, and in ^{86,88,90,92,94}Ge there is triaxial minimum with $\beta = 0.25$ and $\gamma = 20, 25, 30, 40, 45$ respectively as we see in table.(3.1).

In Fig. 3.5, and table 3.2 DD-PC1 results are presented, and no significant difference from the results obtained with NL3* was found, expect the different in

TABLE 3.1: Location of the two ground state minima indicated by (β^0, γ^0) for Ge isotopes using NL3* parameterization. The first minimum is the deepest minimum

Nucleus	first minimum (β^0, γ^0)	second minimum (β^0, γ^0)	Δ E
^{66}Ge	(0.25,60°)	(0.25,45°)	0.56
^{68}Ge	(0.3,55°)	–	–
^{70}Ge	(0.2,60°)	–	–
^{72}Ge	(0.00,0°)	(0.2,60°)	0.18
^{74}Ge	(0.25,30°)	–	–
^{76}Ge	(0.2,0°)	–	–
^{78}Ge	(0.2,0°)	–	–
^{80}Ge	(0.15,0°)	–	–
^{82}Ge	(0.00,0°)	–	–
^{84}Ge	(0.15,0°)	–	–
^{86}Ge	(0.25,20°)	–	–
^{88}Ge	(0.25,25°)	–	–
^{90}Ge	(0.25,30°)	(0.25,60°)	–
^{92}Ge	(0.25,40°)	–	–
^{94}Ge	(0.25,45°)	–	–

TABLE 3.2: As table (3.1), but using DD-PC1 parameterization. The first minimum is the deepest minimum

Nucleus	first minimum (β^0, γ^0)	second minimum (β^0, γ^0)	Δ E
^{66}Ge	(0.25,60°)	(0.25,45°)	1.78
^{68}Ge	(0.25,55°)	–	–
^{70}Ge	(0.20,60°)	–	–
^{72}Ge	(0.00,0°)	(0.20,60°)	2.82
^{74}Ge	(0.25,30°)	–	–
^{76}Ge	(0.20,0°)	–	–
^{78}Ge	(0.2,0°)	–	–
^{80}Ge	(0.15,0°)	–	–
^{82}Ge	(0.00,0°)	–	–
^{84}Ge	(0.20,0°)	–	–
^{86}Ge	(0.25,20°)	–	–
^{88}Ge	(0.25,25°)	–	–
^{90}Ge	(0.25,30°)	(0.25,60°)	0.08
^{92}Ge	(0.25,40°)	–	–
^{94}Ge	(0.25,45°)	–	–

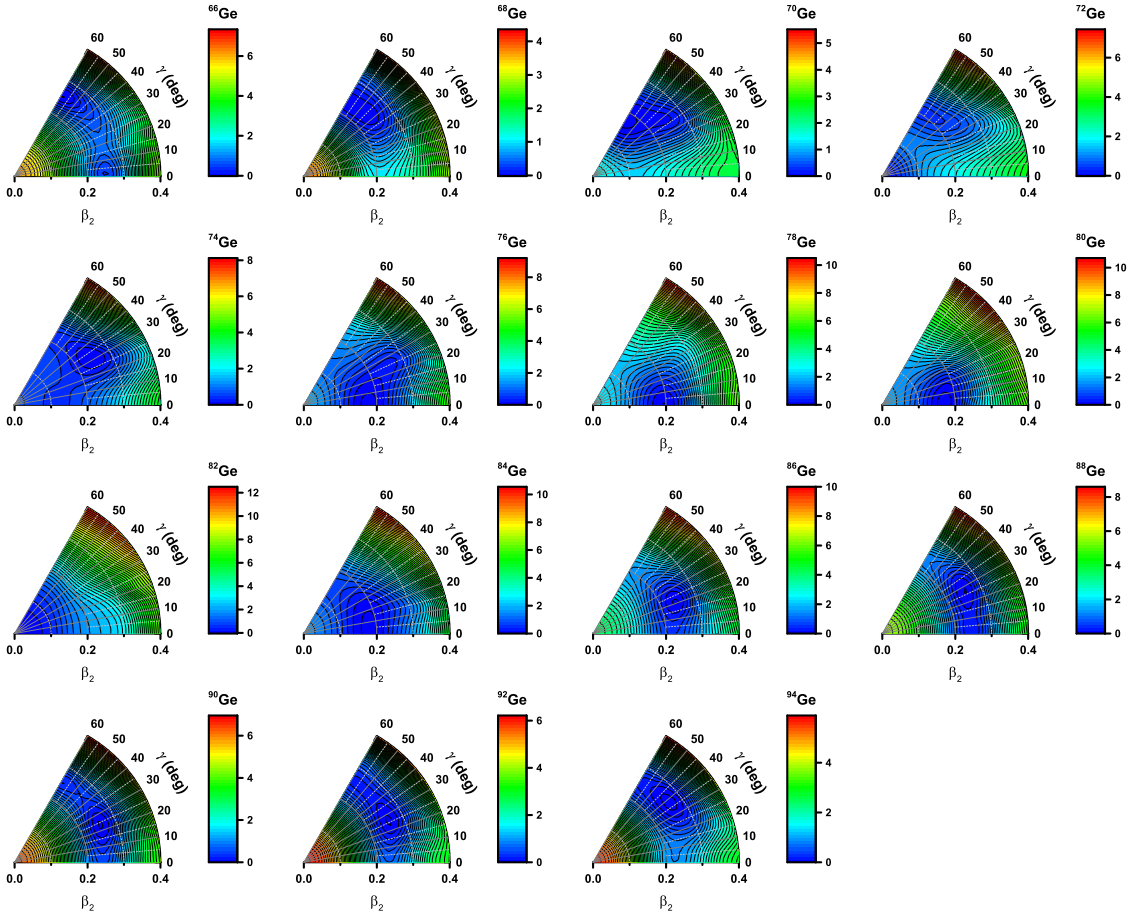

FIGURE 3.5: Similar to Fig. 3.4, but within DD-PC1 parametrization

energy between two minima in ^{66,72,90}Ge. This difference will not affect the binding energy, and the binding energy per nucleon, but will differently affect the two neutron separation energy, neutron, and proton radii as will be shown later. As we see in pervious tables the ground state shape is found to be both oblate and prolate ^{66}Ge, spherical and oblate for ^{72}Ge and triaxial and oblate for ^{90}Ge.

Also the shape of ground state are presented within interacting boson model (IBM) based on Gogny - D1M parametrization taken from [46] and shown in table3.3. It shows that ^{66}Ge has two minima (oblate with $\beta = 0.25$ and triaxial with $\beta = 0.25$, and $\gamma = 45$). The triaxial minimum is the global. The shape of ground state in ^{68}Ge become a triaxial, and it is minimum at $\beta = 0.25$, and $\gamma = 45$. One can see there is a soft change in the ground state deformation. In ^{70}Ge the minimum is an oblate at $\beta = 0.2$, then the shape of ground state has two minima, one of them is spherical, and the other one is an oblate minima at $\beta = 0.2$. The spherical is the deepest minima. In ^{74}Ge there is a triaxial minimum at $\beta = 0.15$, and $\gamma = 45$. For ^{76,78,80,84,86,88}Ge as the same calculations from NL3*, and DD-PC1, the global minimum is a prolate and the value of β_2 is decreasing from 0.25 to 0.15 leading to a spherical shape for ^{82}Ge. Finally, the shape of ground state has two minima differ minima from NL3*, and DD-PC1, the deepest one is an oblate at $\beta = 0.2$, and the other one is a prolate minimum at $\beta = 0.2$, then the shape is change in soft to triaxial minimum at $\beta = 0.25$, and $\gamma = 35, 45$ in ^{90,92}Ge respectively.

TABLE 3.3: As table (3.1), but using IBM based on D1M parameterizations taken from [46]

Nucleus	first minimum (β^0, γ^0)	second minimum (β^0, γ^0)
^{66}Ge	(0.25,55°)	(0.25,0°)
^{68}Ge	(0.25,50°)	–
^{70}Ge	(0.2,60°)	–
^{72}Ge	(0.00,0°)	(0.2,60°)
^{74}Ge	(0.15,45°)	–
^{76}Ge	(0.15,0°)	–
^{78}Ge	(0.2,0°)	–
^{80}Ge	(0.15,0°)	–
^{82}Ge	(0.00,0°)	–
^{84}Ge	(0.15,0°)	–
^{86}Ge	(0.2,0°)	–
^{88}Ge	(0.25,0°)	–
^{90}Ge	(0.25,60°)	(0.2,0°)
^{92}Ge	(0.25,35°)	–
^{94}Ge	(0.25,40°)	–

3.2 Physical properties

Physical properties are often referred to as observables that can be measured experimentally, such as binding energy, two neutron separation energy, neutron, proton, and charge radii. The binding energy is calculated from axial symmetry, and triaxial symmetry, while neutron, proton, and charge radius are calculated from triaxial symmetry.

3.2.1 Binding and two neutron separation energies

Binding energy is defined as the minima energy needed to put the nucleons together. In Fig. 3.6, we have plotted the binding energy corresponding to the ground state of the Ge isotopes whether it is prolate or oblate. For both prolate and oblate shapes, the results are independent from the choice of parameterizations. However, there is one main deviation at ^{72}Ge, where the DD-PC1 results shows higher value of binding energy. This deviation is due to the sudden transition from oblate in ^{72}Ge to a flat minima (In axial calculations), which appears as triaxial minima from triaxial calculations in ^{74}Ge. In general, there is a very good agreement between our results and the results obtained with D1S [52], so for ^{68}Ge to ^{78}Ge D1S has very close values from our calculated energies, and after ^{80}Ge

there is small deviations between our results and the results obtained from D1S, this difference increase as well as the neutron number is increased. The theoretical binding energies within NL3*, DD-ME2, DD-PC1, and D1S parameterizations are in agreement with experimental data [52].

In Fig. 3.7, and 3.8 the binding energy is plotted as a function of mass number. It was obtained from triaxial calculations, and corresponding to prolate, oblate, and triaxial minima. As we see before, there are some nuclei have a flat minima in axial calculation such as ^{72,74,78}Ge. We can not determined the binding energies for these nuclei in axial symmetry, but the triaxial calculations predict it is binding energies.

In Fig. 3.9 the binding energy per mass number (A) is plotted as a function of neutron number. It was obtained from triaxial calculations, and corresponding to global minima. The results are independent from the choice of parameterizations. That is mean there is no main deviation between NL3* and DD-PC1 calculations. The theoretical values from NL3*, and DD-PC1 parameterizations agree with experimental data from [74] with small deviation, and this deviation does not exceed 1 Mev.

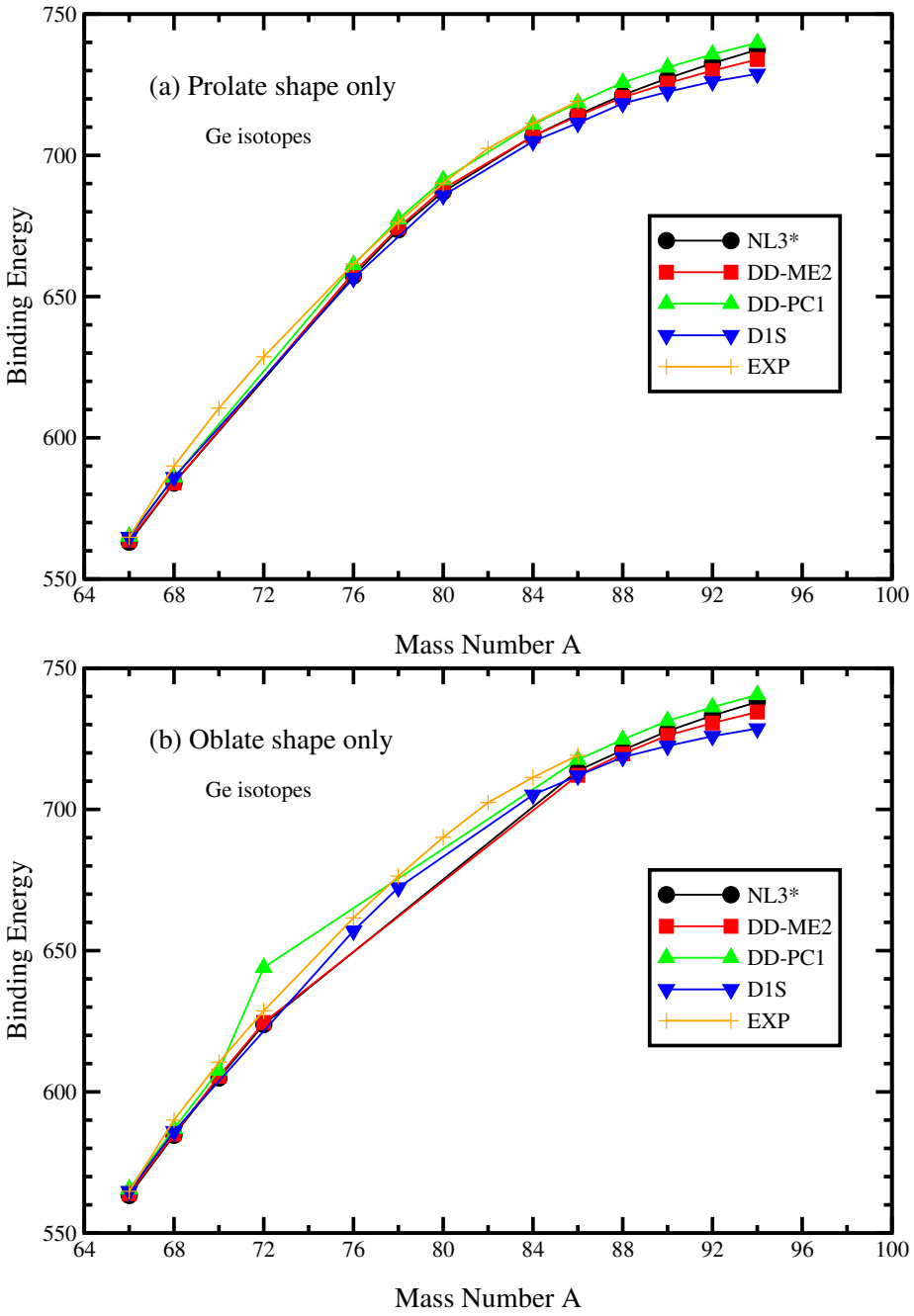

FIGURE 3.6: Binding energy for even-even Ge isotopes in axial symmetry using NL3* (Circles), DD-ME2 (Squares), DD-PC1 (Up triangle) , D1S [52] (Down triangle), and Experimental data (Plus) [52] as a function of mass number (A)

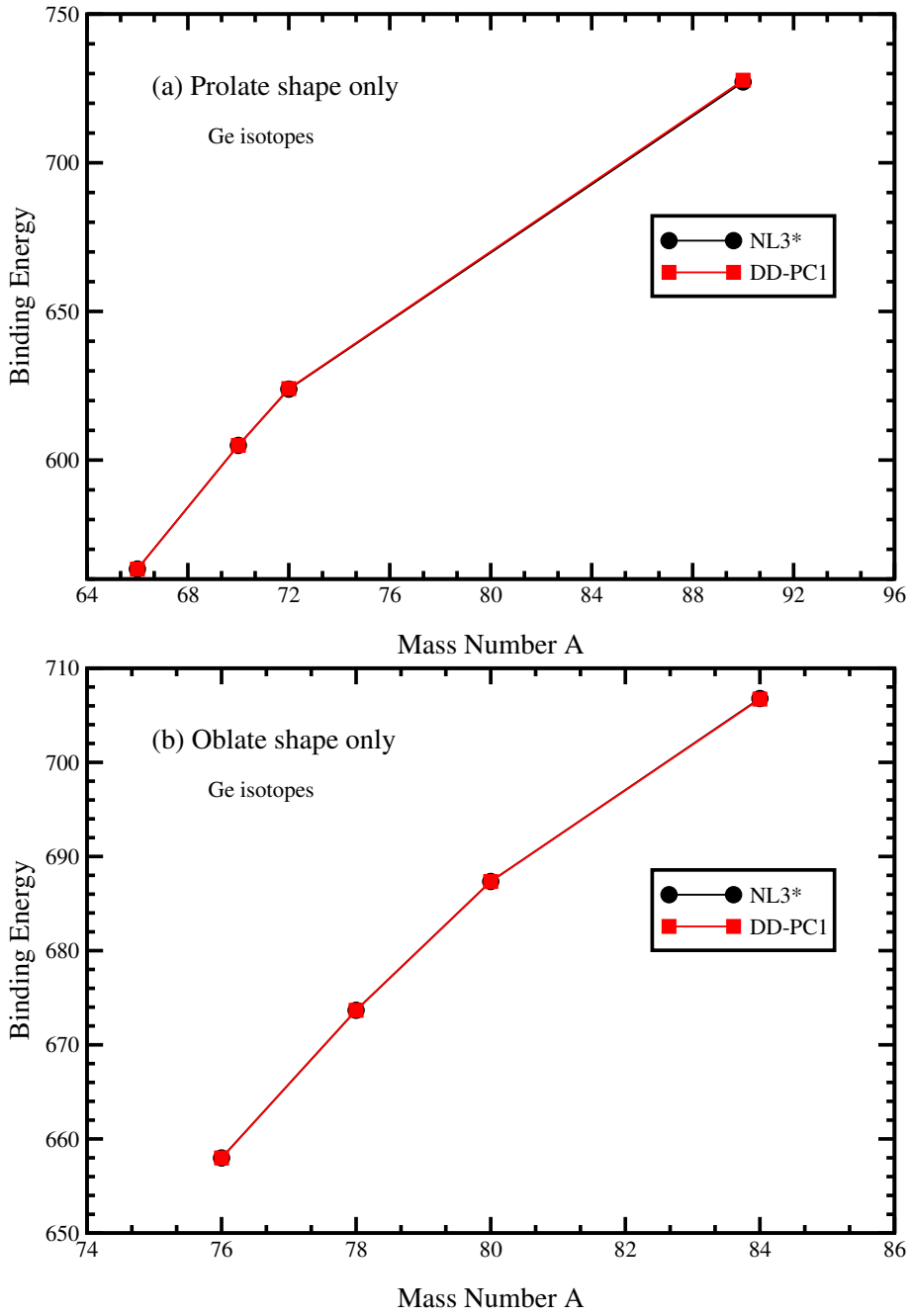

FIGURE 3.7: Binding energy for even-even Ge isotopes in triaxial symmetry for prolate, and oblate minima using NL3* (Circles), DD-PC1 (Up triangle) as a function of mass number (N)

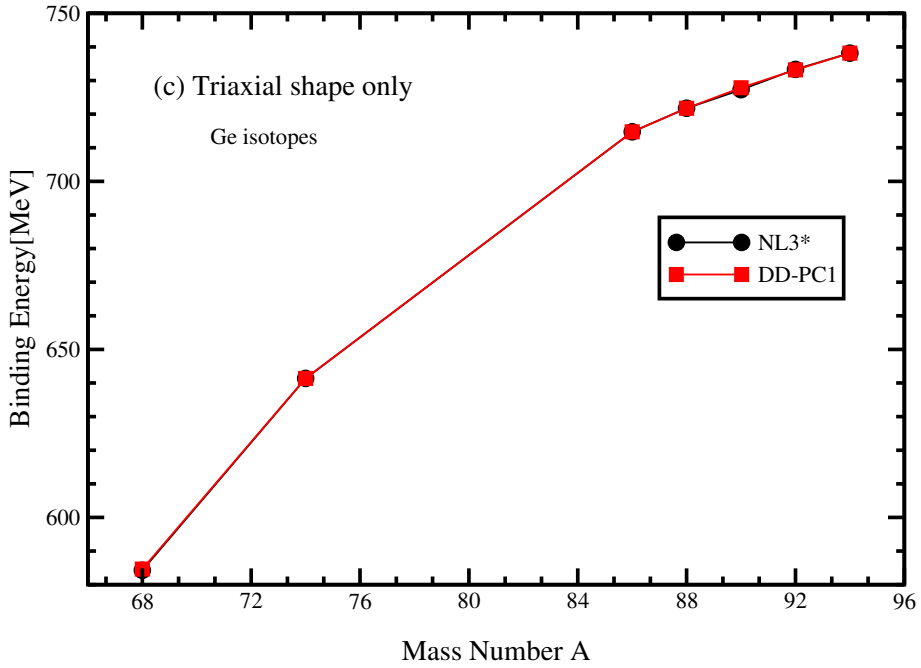

FIGURE 3.8: Binding energy for even-even Ge isotopes in triaxial symmetry for triaxial minima using NL3* (Circles), DD-PC1 (Up triangle) as a function of mass number (N)

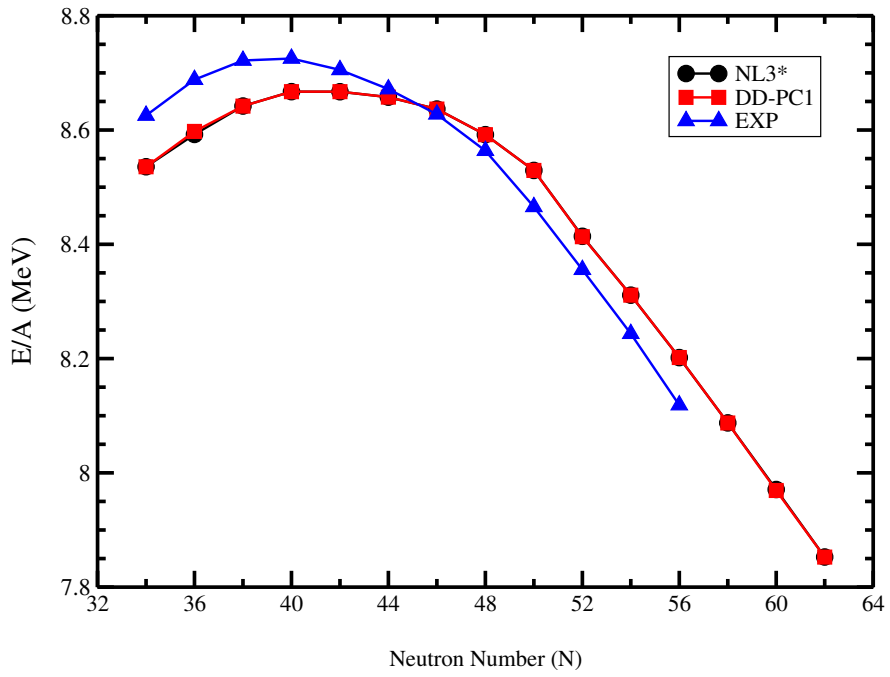

FIGURE 3.9: Binding energy per A for even-even Ge isotopes in triaxial symmetry using NL3* (Circles), DD-PC1 (Squares) , and Experimental data (Up triangle) [52] as a function of neutron number (N)

The two neutrons separation (S_{2n}) is the energy needed to remove two neutrons from a nucleus, and it is given by :

$$S_{2n}(N) = BE({}^{A}_{Z}X_{N}) - BE({}^{A}_{Z}X_{N-2}) \tag{3.1}$$

The two neutron septation energy is plotted as a function of neutron number(N) in Fig. 3.10. One can notice a smooth change in S_{2n} with N, expect for $N = 50$, where we can see a sharp change in S_{2n}. This sharp jump can be attributed to two factor: The first one is due to the magic number $N = 50$, which as we know that separation energy increase near magic numbers. The second factor is the sudden change in the ground state shape from prolate in ^{76,78,80}Ge ($N = 46, 48, 50$) to spherical in ^{82}Ge (N=52). There is good agreement between our calculations and the results obtained in experiments [74].

3.2.2 Neutron, proton and charge radius

Fig. 3.11 show that the radius of neutron and proton obtained from NL3*, and DD-PC1 parameterizations are agreement with each other with small deviation. One can notice there is no significant difference between the radius of neutron, and proton obtained from NL3*, and DD-PC1. However there is a sharp change

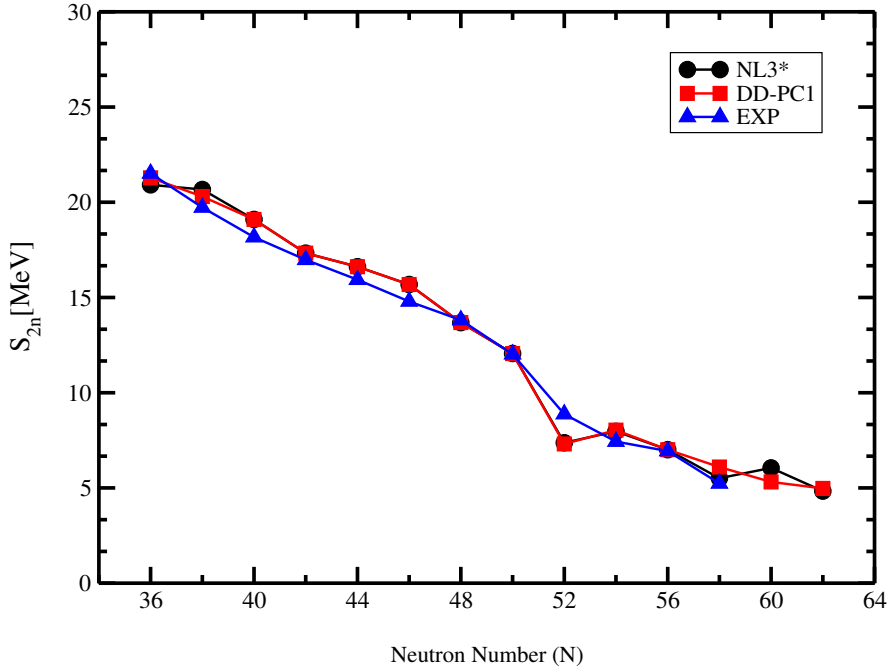

FIGURE 3.10: Two separation energy for even-even Ge isotopes using NL3* (Circles), DD-PC1 (Squares) , and experimental data [74] (Up triangle) as a function of neutron number (N)

in both neutron radius (R_n), and proton radius (R_p) at N=50. This sharp can be attributed to the sudden transition from from spherical in ^{82}Ge (N=50) to deformed shape in ^{84}Ge (N=52). Also one can see that a sudden transition from spherical shape in the ground state to triaxial shape at N=42 is reflected in a sharp change in the radius of proton.

NL3* predicts larger values of R_p compared with the once obtained using DD-PC1 at N=36. This difference coming from the different location of the ground state minimum. This ground state has triaxial minimum with $\beta = 0.3$, and $\gamma = 55$ by NL3*, whereas DD-PC1 predicts it has triaxial minimum with $\beta = 0.25$, and $\gamma = 55$.

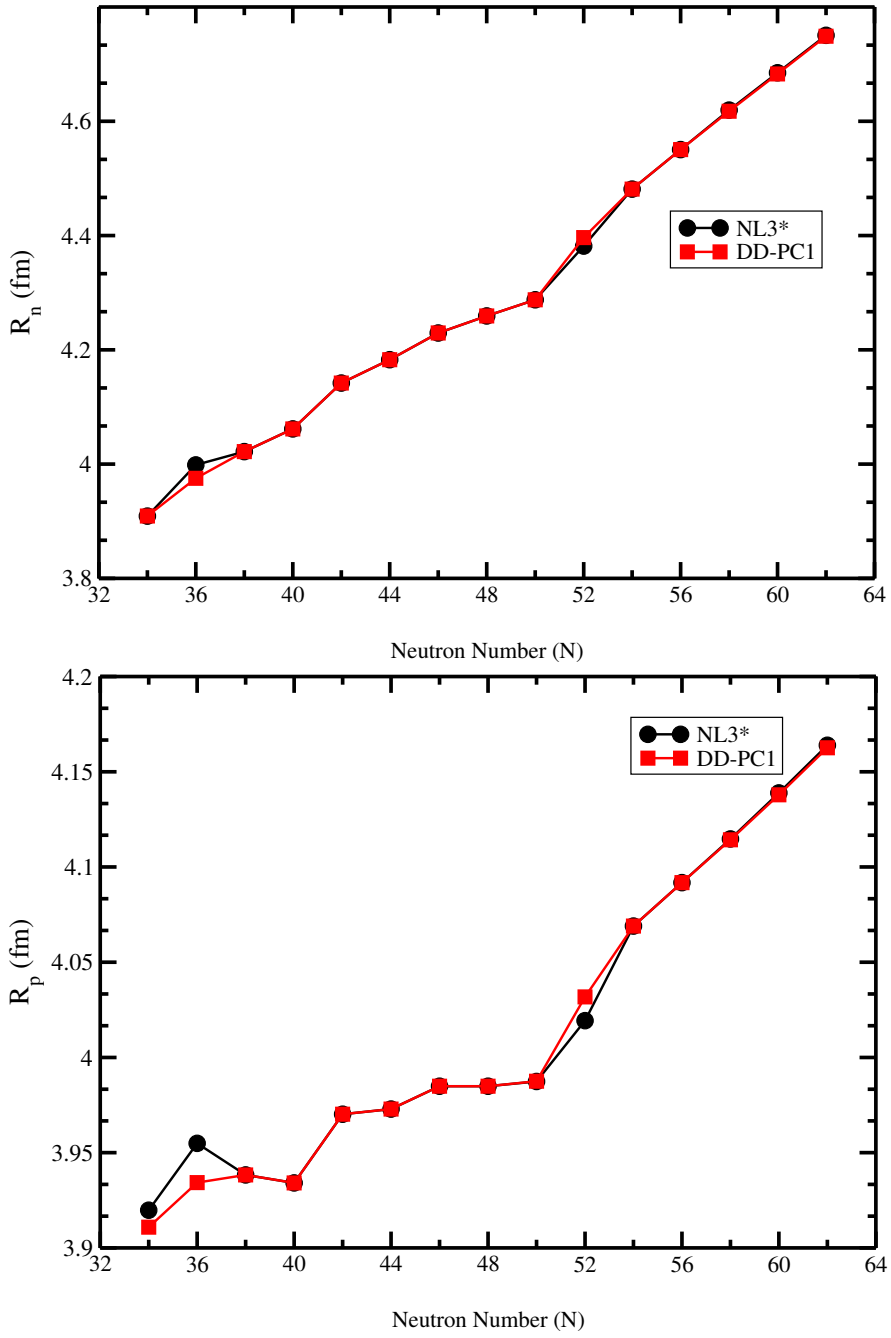

FIGURE 3.11: Radius of neutron, and Proton for even-even Ge isotopes using NL3* (Circles), DD-PC1 (Squares) , as a function of neutron number (N)

One of the most fundamental properties of atomic nuclei is the nuclear charge radius. It plays a key role in studying the characters of nucleus and testing theoretical models of nuclei. It is calculated by this formula :

$$R_c = \sqrt{R_p^2 + 0.64} \tag{3.2}$$

Where is 0.64 is related to the finite volume of the proton (volume correction).

Fig. 3.12 show the charge radius for Ge isotopes. One can notice because there is a smooth transition in the ground state deformation at $N = 44$ to $N = 62$ will be seen as a smooth evolution for R_c. On the other hand, a sharp change in the R_c at $N = 36$, $N = 42$ and $N = 52$. This sharp attributed to a sudden change of ground state shape from prolate at $N = 34$ to triaxial shape at $N = 36$, also a sudden change from spherical at N=40 to deformed shape (triaxial) at $N = 42$. Moreover, there is a sudden transition in the shape of ground state from spherical in ^{82}Ge ($N = 50$) to deformed shape in ^{84}Ge ($N = 52$). The charge radius obtained from NL3* are agreement with ones from DD-PC1, expect at $N = 36$. One can see that the value of charge radius of proton (R_c) change suddenly at $N = 36$ by NL3*, whereas it is change smoothly by DD-PC1. This change suddenly referred to same reason of proton sharp change suddenly.

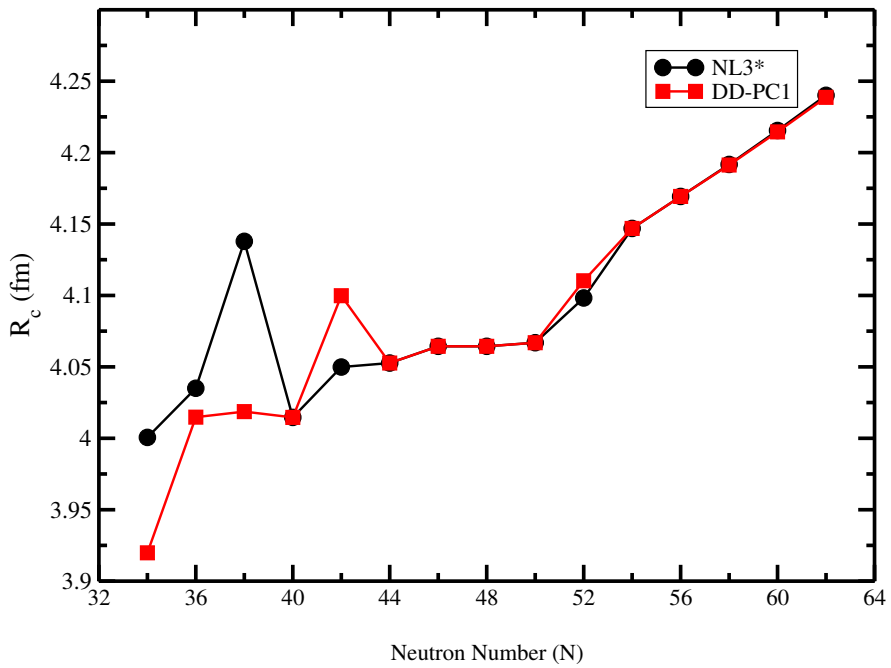

FIGURE 3.12: Charge Radius of for even-even Ge isotopes using NL3* (Circles), DD-PC1 (Squares) , as a function of neutron number (N)

Chapter 4

Se isotopes

In this chapter we will analyze the same calculations as we did in pervious chapter, but for even-even Se (Z = 34, $34 \leqslant N \leqslant 62$) isotopes. The axial calculations are performed using NL3*, DD-ME2, and DD-PC1 parameterizations, while the triaxial calculations are performed using NL3*, and DD-PC1 parameterizations.

4.1 Potential energy surface

In this section we perform constrained calculations on β (Eq. 2.68) and γ (Eq.2.70), and obtain the potential energy curves in axial, and triaxial calculations for Se isotopes. The results are compared with potential energy curves obtained from relativistic Hartree-Fock-Bogolibouve within Gogny- D1S [52], and potential

energy surfaces obtained from interacting bosons model (IBM) based on Gogny-D1M [46].

4.1.1 Axial symmetry

From potential energy curves (PEC) calculations shown in Figs. 4.1, and 4.2 one can see that these isotopes can be classified into three categories. The first category contains isotopes that has only one minimum, namely ^{80,82,84}Se. ^{80}Se has a prolate minimum at $\beta = 0.2$, and similarly in ^{82}Se there is a prolate minimum at $\beta = 0.15$, however, the prolate minimum less pronounced. Then the shape of ground state becomes a spherical in ^{84}Se. The second category contains isotopes that has two minima, namely ^{68,70,78,88,90,92,94,96}Se. ^{68,70}Se have a two minima (prolate and oblate)at $|\beta| = 0.25$, it is similarly in ^{76,78}Se there are two minima, one of them is a prolate at $\beta = 0.2$, and the other minima is an oblate at $\beta = 0.15$, also the shape of ground state has a prolate and oblate with minima at $|\beta| = 0.2$ in ^{88}Se, and in ^{90,92,94,96}Se have a prolate and oblate with minima at $|\beta| = 0.25$. The third category contains isotopes that has flat minima such as ^{74,86}Se. Finally, ^{72}Se may be has one minima or flat, and this minima could be a

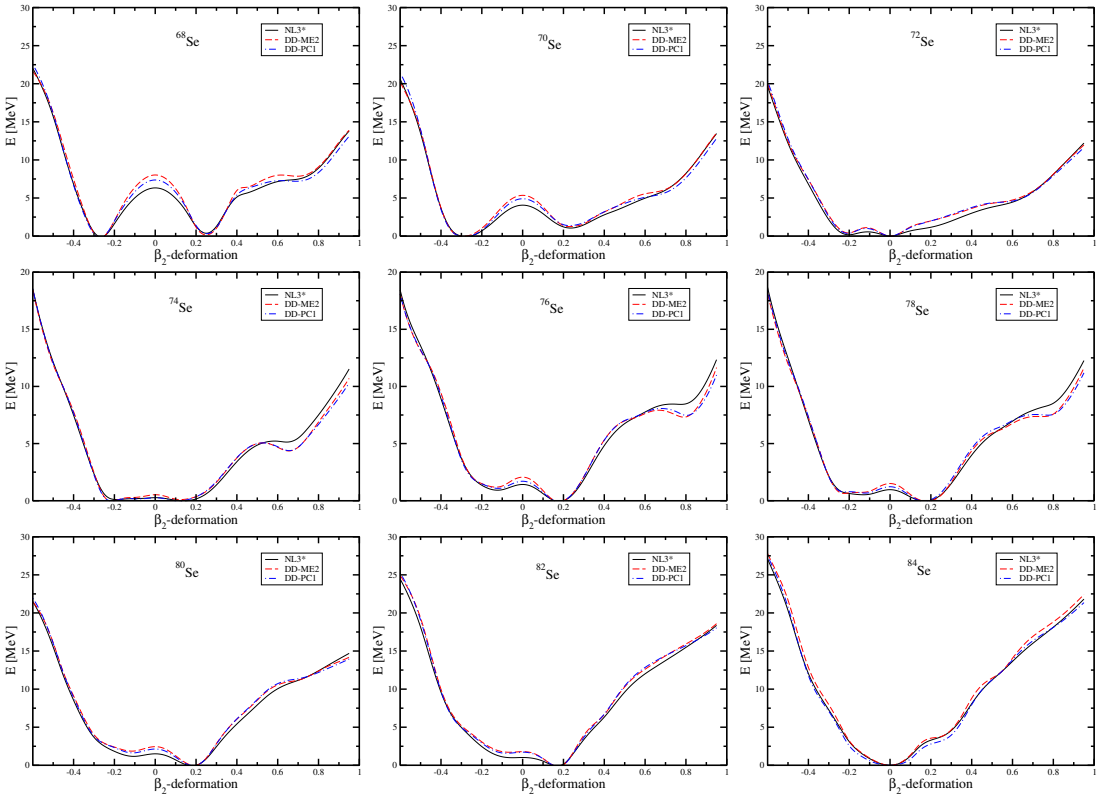

FIGURE 4.1: Similar to Fig. 3.1, but for even-even Se isotopes from neutron number $34 \leqslant N \leqslant 50$

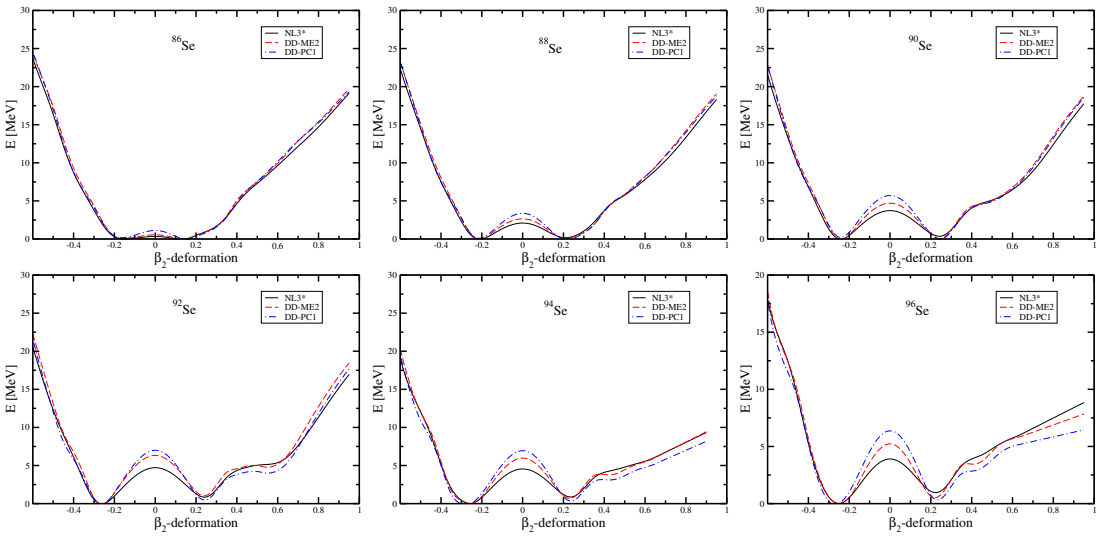

FIGURE 4.2: Similar to Fig. 4.1, but from neutron number $52 \leqslant N \leqslant 62$

prolate or oblate.

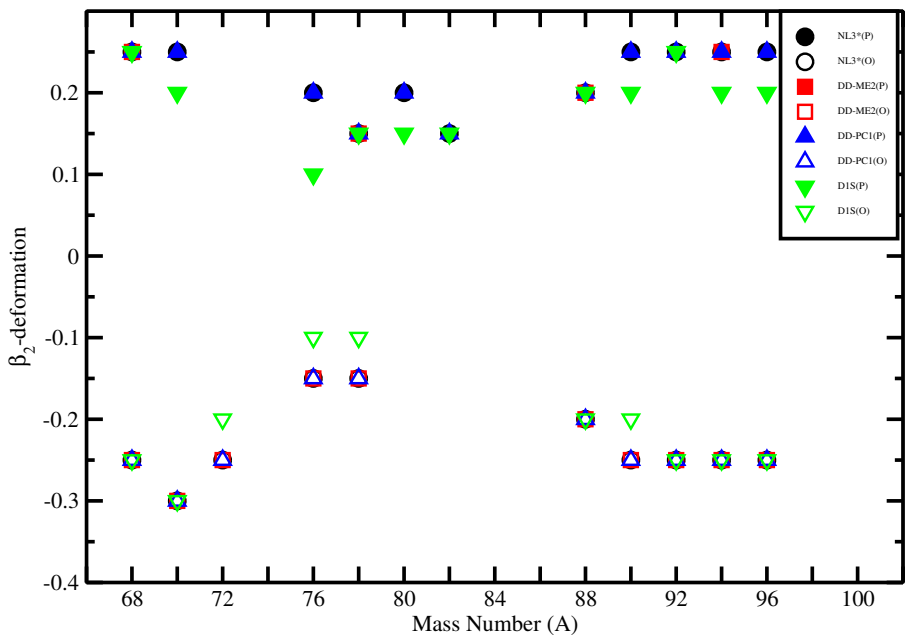

FIGURE 4.3: Similar to Fig. 3.3, but for Se isotopes

In Fig. 4.3 we show the ground state deformation for all categories extracted from Figs.4.1, and 4.2, and for D1S in taken from ref. [52]. Both prolate and oblate minima obtained from NL3*, DD-ME2 and DD-PC1 parametrization agree with the results obtained from D1S in [52] with small deviation in the location of their minima. For example our calculations predict a prolate minima with $\beta = 0.2$ in ^{76}Se, whiles D1S predicts a prolate minima with $\beta = 0.1$.

4.1.2 Triaxial symmetry

Fig 4.4, and table.3.1 shown ^{68,70,74}Se have two minima, both of these minima is axial. In ^{68}Se one of them is oblate with $\beta = 0.25$ and the other is prolate with

$\beta = 0.25$, and the energy difference between them equal 0.37 MeV. In ^{70}Se the first minimum is oblate with $\beta = 0.3$, and the other minimum is prolate with $\beta = 0.25$. The deepest minimum is the oblate. In ^{74}Se the deepest minimum is an oblate with $\beta = 0.2$, and the other minimum is spherical, with energy difference between them 0.27 MeV. The shape of ground state has one minimum in ^{72,76,78,80,82,84,86}Se, this minimum is prolate at $\beta = 0.25$ in ^{72}Se, and it is an oblate in ^{76,78,80,82,86}Se with different β varying from 0.15 to 0.2. In ^{84}Se the shape of ground state becomes suddenly spherical. However, the shape of ground state has two minima in ^{88}Se , the deepest one is an oblate with $\beta = 0.2$, and the other is a prolate with $\beta = 0.2$. Finally, in ^{90,92,94,96}Se there is two minima, the deepest one is a prolate minima with $\beta = 0.25$, and the other minima is an oblate with $\beta = 0.25$.

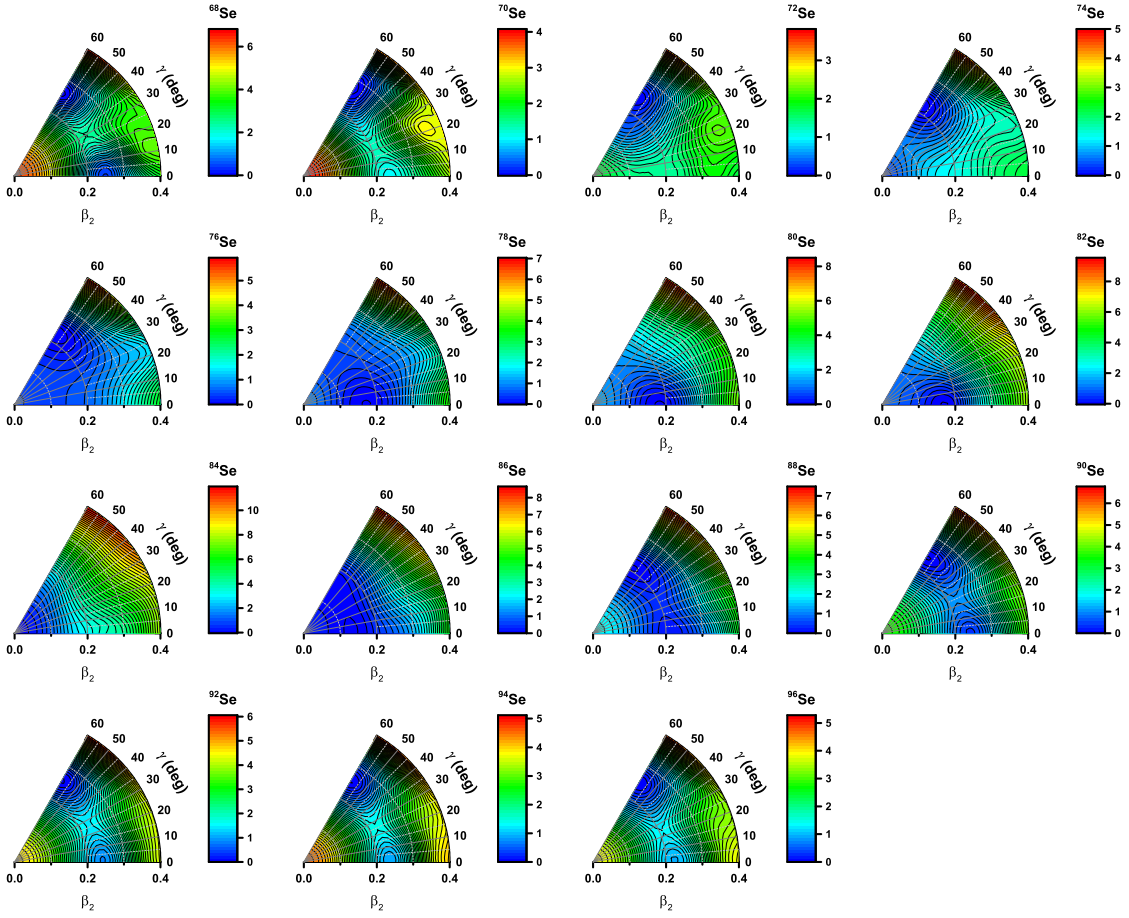

FIGURE 4.4: Similar to Fig. 3.4, but for Se isotopes using NL3*

TABLE 4.1: Location of the two ground state minima indicated by (β^0, γ^0) for Se isotopes using NL3* parameterization. The first minimum is the deepest minimum

Nucleus	first minimum (β^0, γ^0)	second minimum (β^0, γ^0)	Δ E
^{68}Se	(0.25,60°)	(0.25,0°)	0.37
^{70}Se	(0.3,60°)	(0.25,0°)	1.07
^{72}Se	(0.25,60°)	–	–
^{74}Se	(0.2,60°)	(0.00,0°)	0.27
^{76}Se	(0.2,60°)	–	–
^{78}Se	(0.15,0°)	–	–
^{80}Se	(0.2,0°)	–	–
^{82}Se	(0.15,0°)	–	–
^{84}Se	(0.00,0°)	–	–
^{86}Se	(0.15,60°)	–	–
^{88}Se	(0.2,60°)	(0.2,0°)	0.18
^{90}Se	(0.25,60°)	(0.25,0°)	0.38
^{92}Se	(0.25,60°)	(0.25,0°)	0.87
^{94}Se	(0.25,60°)	(0.25,0°)	0.92
^{96}Se	(0.25,60°)	(0.25,0°)	1.10

Fig. 4.5, and table. 4.2 shown the minima of ground state by DD-PC1 parametrization, and it is agreement with the results from NL3* calculations, expect in ^{86,88,90}Se. NL3* predicts only a prolate minimum for the ground state in ^{86}Se, but DD-PC1 shown there is two minima, one of them is prolate with $\beta = 0.15$, and the other is an oblate with $\beta = 0.15$. The oblate minimum is the deepest one. In ^{88}Se the deepest minimum obtained from NL3* is prolate with $\beta = 0.2$, whiles the deepest minimum obtained from DD-PC1 is an oblate minimum with $\beta = 0.2$. In ^{90}Se, both parameterizations (NL3*, and DD-PC1) predicts two minima for the ground state shape, but the absolute minima obtained from NL3* it is

a prolate, and it is an oblate by DD-PC1. Also NL3* predict the energy difference between two minima in ^{68,70,74,88,90,92,94}Se are 0.37, 1.07, 0.27, 0.18, 0.38, 0.87, 0.92, 1.10 MeV respectively, but DD-PC1 predict it is 0.33, 1.42, 0.08, 0.14, 0.24, 0.55, 0.40, 0.01 MeV. This difference affect the binding energy per nucleon, two neutron separation energy, neutron, and proton radius as will be shown later.

As we notice in Table. 4.3 the minima investigated within interacting boson model (IBM) based on Gogny-D1M parametrization taken from [46] are agreement with our results, with small difference in the location of minima, and it shows that ^{68,70}Se has two minima (oblate with $\beta = 0.25$ and prolate with $\beta = 0.25$). The oblate minimum is the global. One can see there is a soft change in the ground state deformation. In ^{72}Ge the minimum is an oblate at $\beta = 0.2$, then the shape of ground state has two minima, one of them is spherical, and the other one is an oblate minimum at $\beta = 0.2$. The spherical is the deepest minimum. In ^{76}Se there is an oblate minimum at $\beta = 0.2$. For ^{78,80,82,86}Se as the same calculations from NL3*, and DD-PC1, the global minimum is a prolate and the value of β_2 is decreasing from 0.20 to 0.15 leading to a spherical shape for ^{84}Se. The shape of ground state has two minima in ^{90,92,94,96}Se. The deepest one is a prolate at $\beta = 0.25$, and the other one is an oblate minimum at $\beta = 0.25$. One can see D1M

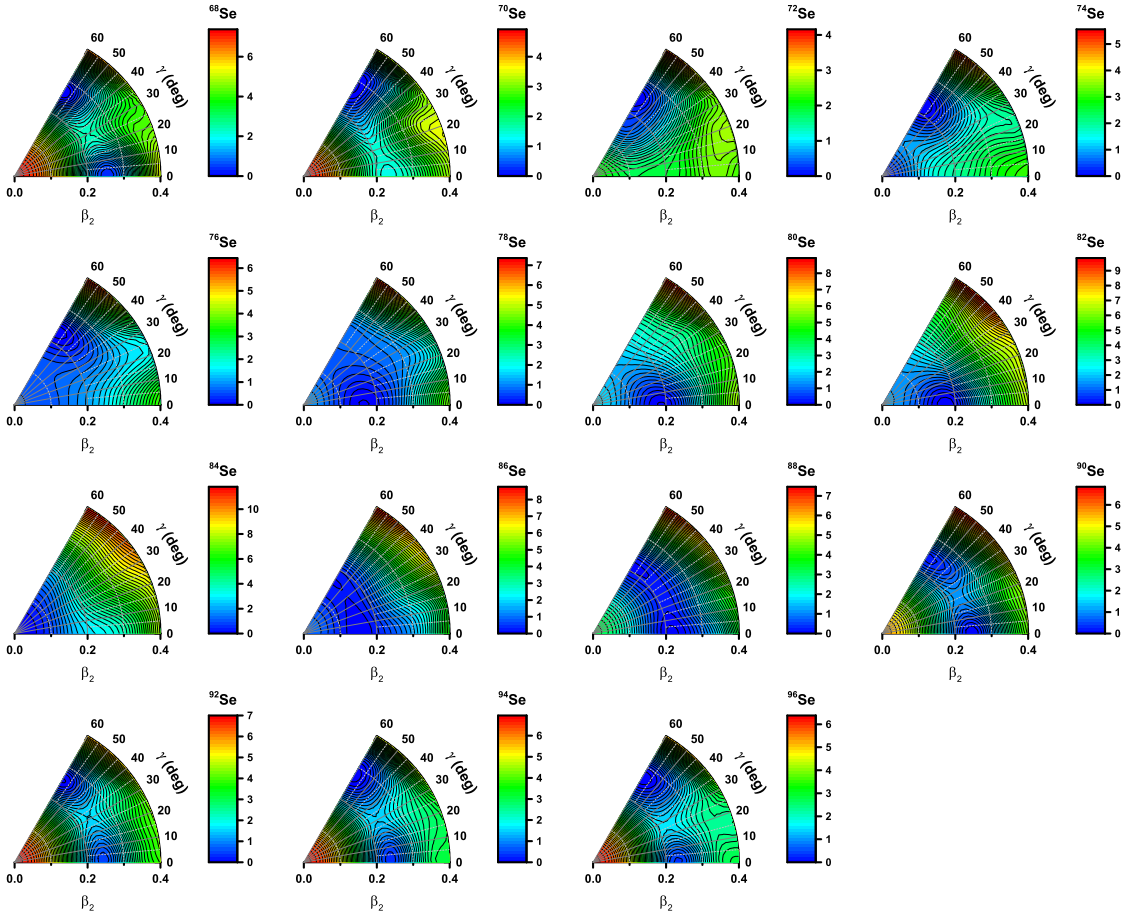

FIGURE 4.5: Similar to Fig. 4.4, but using DD-PC1 parametrization

predicts triaxial minimum at $\beta = 0.2$, and $\gamma = 25$ in ^{84}Se, while our calculations predict the ground state has two minima (prolate and oblate).

The coexistence of two different shapes for Se isotopes in the ground state is better seen as compared with Ge isotopes. It is clearly seen at the neutron deficient and neutron rich sides of the isotopic chain. In the rest of the nuclei, the shape is either oblate or spherical.

TABLE 4.2: As table 4.1, but using DD-PC1 parameterization

Nucleus	first minimum (β^0, γ^0)	second minimum (β^0, γ^0)	Δ E
^{68}Se	(0.25,60°)	(0.25,0°)	0.33
^{70}Se	(0.30,60°)	(0.25,0°)	1.42
^{72}Se	(0.25,60°)	–	–
^{74}Se	(0.25,60°)	(0.00,0°)	0.08
^{76}Se	(0.25,60°)	–	–
^{78}Se	(0.15,0°)	–	–
^{80}Se	(0.2,0°)	–	–
^{82}Se	(0.15,0°)	–	–
^{84}Se	(0.00,0°)	–	–
^{86}Se	(0.15,0°)	(0.15,60°)	0.19
^{88}Se	(0.2,0°)	(0.20,60°)	0.14
^{90}Se	(0.25,0°)	(0.25,60°)	0.24
^{92}Se	(0.25,60°)	(0.25,0°)	0.55
^{94}Se	(0.30,60°)	(0.25,0°)	0.40
^{96}Se	(0.25,60°)	(0.25,0°)	0.01

TABLE 4.3: As table 4.1, but using DIM parameterization taken from [46]

Nucleus	first minimum (β^0, γ^0)	second minimum (β^0, γ^0)
^{68}Se	(0.25,60°)	(0.25,0°)
^{70}Se	(0.25,60°)	(0.25,0°)
^{72}Se	(0.25,60°)	–
^{74}Se	(0.2,60°)	(0.00,0°)
^{76}Se	(0.2,60°)	–
^{78}Se	(0.15,0°)	–
^{80}Se	(0.15,0°)	–
^{82}Se	(0.15,0°)	–
^{84}Se	(0.00,0°)	–
^{86}Se	(0.15,0°)	–
^{88}Se	(0.2,25°)	–
^{90}Se	(0.25,60°)	(0.25,0°)
^{92}Se	(0.25,60°)	(0.2,0°)
^{94}Se	(0.25,60°)	(0.2,0°)
^{96}Se	(0.25,60°)	(0.2,0°)

4.2 Physical properties

One can relate the shape evolution of ground state seen in the pervious section with the change in the value of several physical properties such as binding energy, two neutron separation energy, neutron, proton, and charge radii. Where the shape of ground state change smoothly this seen as smooth evolution of the physical properties. On other hand, when the shape change suddenly this reflected as a sharp jump in these properties. The binding energy in calculated from axial symmetry, and triaxial symmetry, while neutron, proton, and charge radius are calculated from triaxial symmetry.

4.2.1 Binding and separation energies

In Fig. 4.6 the value of binding energy obtained from NL3*, and DD-PC1 are agree with the results obtained from D1S parametrization [52]. One can notice there is no a sharp jump in the binding energy values, so the sudden change in the ground state deformation do not affects the binding energy. Our calculations are agreement with the experimental data [52].

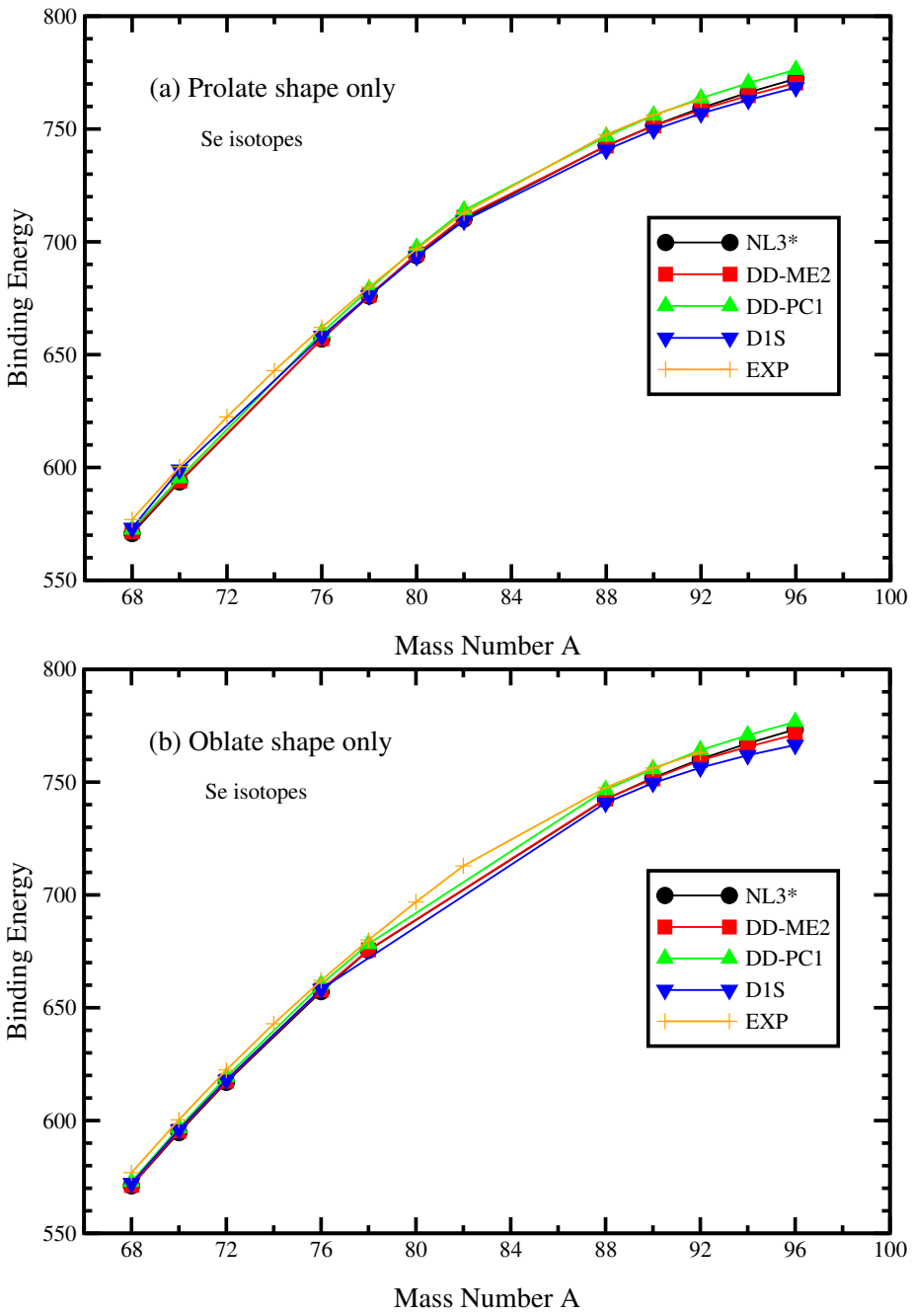

FIGURE 4.6: Similar to Fig. 4.6, but for Se isotopes

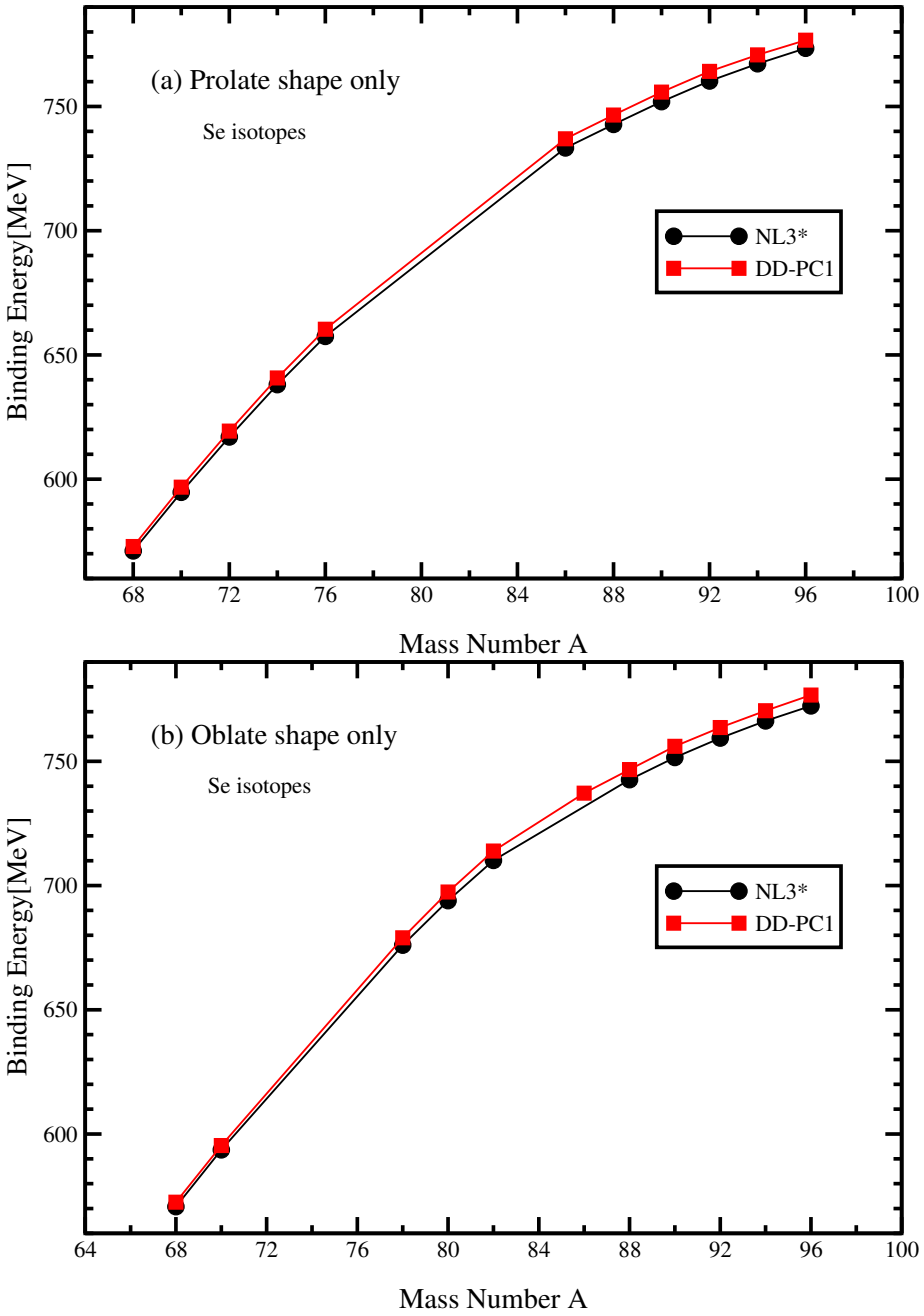

FIGURE 4.7: Binding energy for even-even Se isotopes in triaxial symmetry using NL3* (Circles), DD-PC1 (Up triangle) as a function of mass number (N)

In Fig. 4.7 the binding energy obtained from triaxial calculations is plotted as a function of mass number. For both prolate and oblate the results are independent from the choice of parameterizations. Also the binding energy obtained from axial symmetry are agree with results obtained from triaxial symmetry.

In Figure. 4.8 the binding energy per mass number (A) obtained from triaxial calculations is plotted as a function of neutron number. There are agreement between the energy obtained from NL3*, and DD-PC1 with small deviations. However, there is three mean deviation at $N = 52, 54, 56$, when the DD-PC1 results shows higher value of binding energy. This deviation coming from the different location of the ground state minimum. The ground state investigated by NL3* has oblate minima, whiles DD-PC1 predicts it has prolate minima. One can notice a sharp change in S_{2n} at N=50. This sharp jump can be attributed to two factor. The first one is due to the magic number N=50. The second factor is the sudden change in the ground state shape from prolate in ^{76,78,80}Se ($N = 46, 48, 50$) to spherical in ^{82}Ge ($N = 52$). The theoretical results obtained from NL3*, and DD-PC1 parametrization are agreement partially with the experimental data [74].

One can see in Fig.4.9 the two neutron separation energy (S_{2n}) for Se isotopes obtained from NL3*, and DD-PC1 are agreement with each other. There is a sharp change in S_{2n} at $N = 50$ can be attributed to two factor. The first one is due to the magic number $N = 50$, which as we know that separation energy increase as near magic numbers. The second factor is the sudden change in the ground state shape from spherical at N=50 to deformed shape at N=52. Our

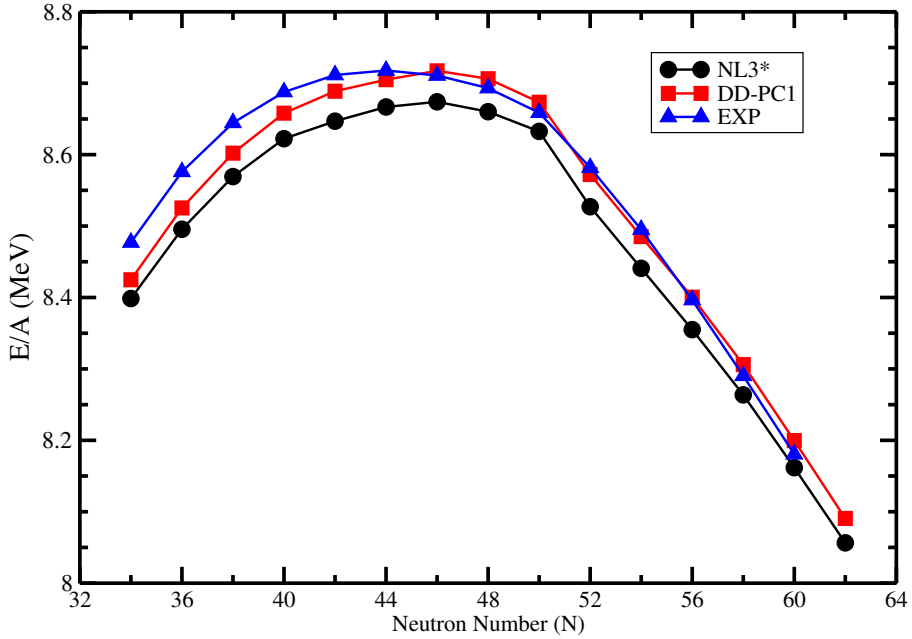

FIGURE 4.8: Binding energy per A for even-even Se isotopes in triaxial symmetry using NL3* (Circles), DD-PC1 (Squares) , and Experimental data (Up triangle) [52] as a function of neutron number (N)

calculations are agreement with experimental data [74].

4.2.2 Neutron, and proton radius

There is a good agreement in Fig. 4.10 for both the radius of neutron and proton obtained from NL3* and DD-PC1 parametrization. However, there is small deviation when the NL3* results shows higher value of neutron radius. On the other hand, the DD-PC1 shows higher value of proton radius. This different attributed to the differs in shape evolution for ground state between NL3* and DD-PC1.

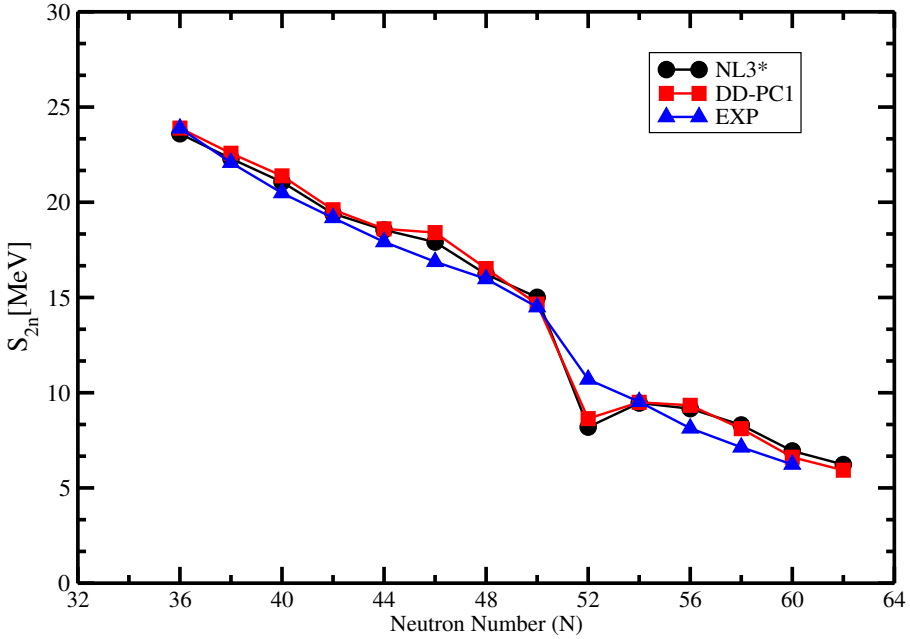

FIGURE 4.9: Two separation energy for even-even Se isotopes using NL3* (Circles), DD-PC1 (Squares) , and experimental data [74] (Up triangle) as a function of neutron number (N)

Fig. 4.11 show the charge radius for Se isotopes. One can see there is a sharp change in the R_c at $N = 52$. This sharp attributed to a sudden change of ground state shape from prolate at $N = 50$ to spherical shape at $N = 52$. Also as we know that the charge proton radius increase as near magic numbers, and $N = 50$ it is a magic number.

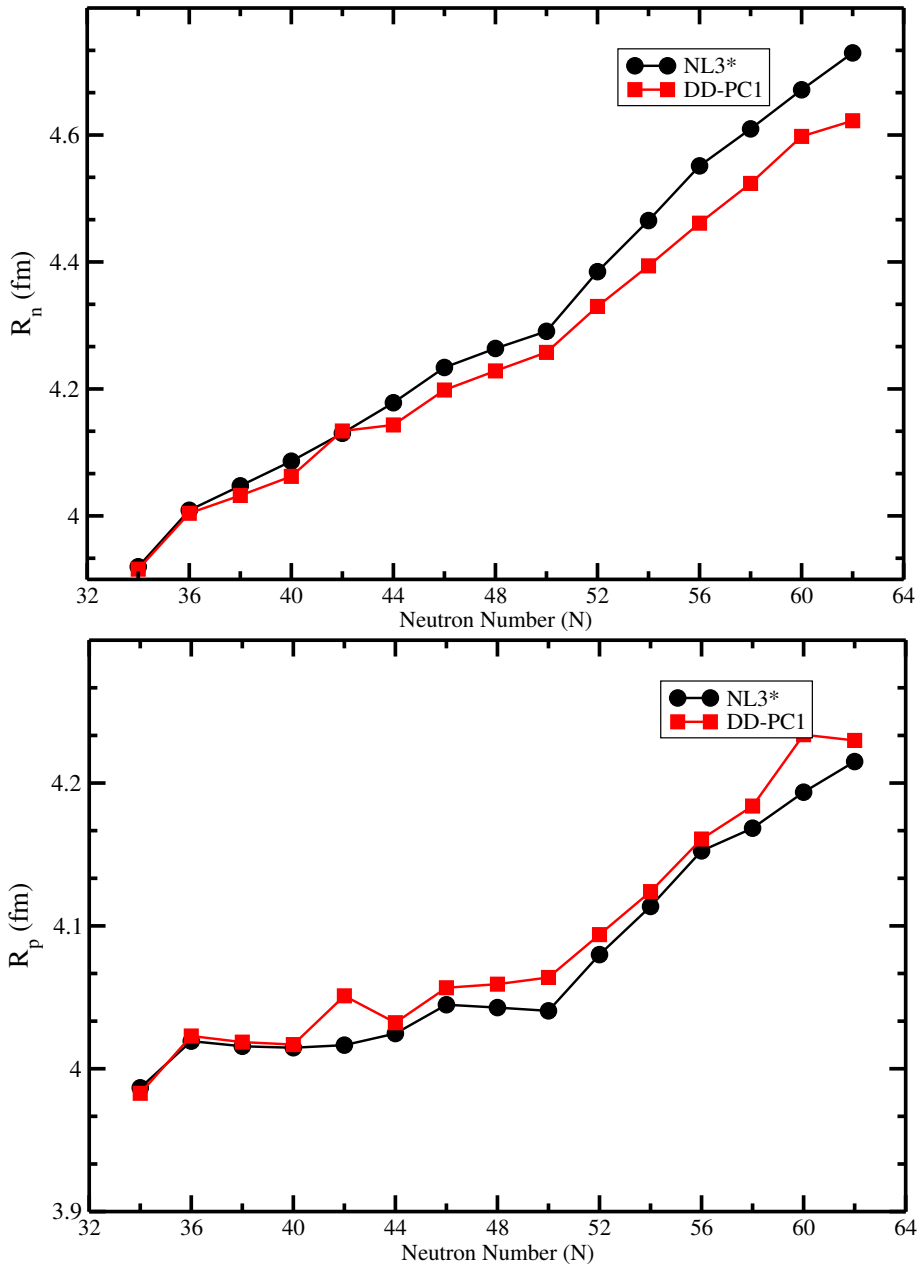

FIGURE 4.10: Radius of neutron, and Proton for even-even Ge isotopes using NL3* (Circles), DD-PC1 (Squares) , as a function of neutron number (N)

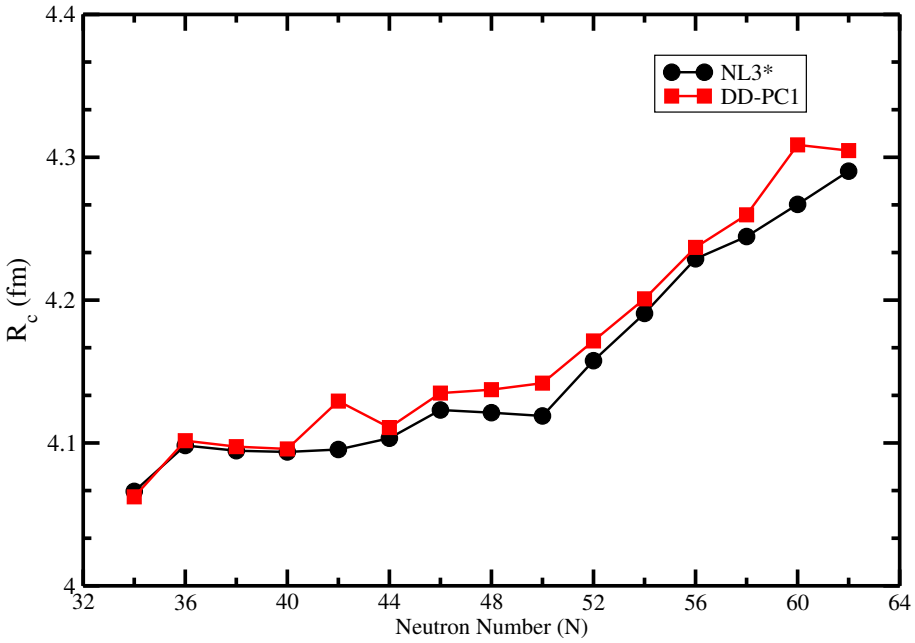

FIGURE 4.11: Charge Radius of for even-even Se isotopes using NL3* (Circles), DD-PC1 (Squares) , as a function of neutron number (N)

Chapter 5

Conclusion

In this thesis relativistic Hartree-Fock-Bogoluibove model (RHFB) has been successfully applied to investigate the shape coexistence and the physical properties such as binding, two neutron separation energies, neutron and proton radii in ground state of Ge (Z = 32, $34 \leq N \leq 62$) isotopes, and Se (Z =34, $34 \leq N \leq 62$) isotopes. The binding energy in calculated from axial symmetry, and triaxial symmetry are agreement with experimental data, and neutron, proton, and charge radius are calculated from triaxial symmetry.

The potential energy curves for Ge and Se isotopes were plotted as a function of deformation parameter β_2 in axial calculations (Prolate shapes corresponding to $\beta_2 > 0$, and oblate shape corresponding to $\beta_2 < 0$). We can notice the energy does

not vary with β_2 in a ceratin region of PEC such as in ^{72,74,78}Ge (flat minima). However, the triaxial potential energy surfaces (PES) predict there are two minima in ^{72}Ge, one of them spherical and the other is an oblate minima, wheals there is one minima in ^{74,78}Ge. This minima it is a triaxial in ^{74}Ge and it is a prolate in ^{78}Ge. Similar plots were also done for Se isotopes. Shape coexistence manifest itself in Se isotopes better than Ge isotopes, both oblate and prolate shapes are found in the ground state for the neutron rich side of the isotopic chain. In the Se isotopes one can see an oblate-prolate shape transition from ^{76}Se to ^{78}Se, and prolate-spherical transition from ^{82}Se to ^{84}Se.

One can see that the smooth change in the ground state deformation is connected with a smooth evolution of the physical properties in the ground state. The sharp jump in most of the physical properties is observed at $N = 50$. This sharp jump is due to the change of the ground state shape in the neighboring nuclei.

Our results are independent from the choice of parametrization, and it is in good agrement with results obtained from other models.

Bibliography

[1] Kris Heyde, John L. Wood, Phys. Rev. Mod 83, 1467 (2011).

[2] H. Abusara, Shakeb Ahmad, and S. Othman, Phys. Rev. C 95, 054302 (2017).

[3] R. Palit, H. C. Jain, P. K. Joshi, J. A. Sheikh, and Y. Sun, Phys. Rev. C 63, 024313 (2001).

[4] J. K. Johansson, D. G. Popescu, D. D. Rajnauth, et al, Phys. Rev. C 40, 132 (1989).

[5] J. D. Richards, T. Berggren, et al, Phys. Rev. C 56, 1389 (1997).

[6] S. K. Chamoli, Rajesh Kumar, et al, Phys. Rev. C 75, 054323 (2007).

[7] J. E. Garcia-Ramos, K. Heyde, Phys. Rev. C 89, 014306 (2014).

[8] J .E. Garcia-Ramos, et al, Phys. Rev. C 89, 034313 (2014).

[9] P.-G. Reinhard, et al, Phys. Rev. C 60, 014316 (1999).

[10] C. A. Grossmann, et al, Phys. Rev. C 62, 024323 (2000).

[11] W. Frank, P. von Brentano, A. Gelberg, and H. Harter, Phys. Rev. C 38, 2358 (1988).

[12] S. Kuyucak, I. Morrison, and T. Sebe, Phys. Rev. C 43, 1187 (1991).

[13] P. G. Reinhard, et al, Phys. Rev. C 60, 014316 (1980).

[14] S. Suchyta, S. N. Liddick, Y. Tsunoda, et al, Phys. Rev. C 89, 021301 (2014).

[15] E. S. Paul, D. B. Fossan, et al, Phys. Rev. C 40, 1255 (1989).

[16] M. O. Kortelahti, E. F. Zganjar, et al, Phys. Rev. C 43, 484 (1991).

[17] J. L. Egido, et al, Phys. Rev. Lett. 93, 082502 (2004).

[18] M. S. Kaplan, et al, Phys. Rev. C 44, 668 (1991).

[19] G. Lhersonneau, et al, Phys. Rev. C 56, 2445 (1997).

[20] Y. Liang, et al, Phys. Rev. C 45, 1041 (1992).

[21] Andreas Gorgen, and Wolfram Korten, Journal of Physics G Nuclear and Particle Physics, 43(2), 024002 (2016).

[22] G. D. Dracoulis, et al, Phys. Rev. C 69, 054318 (2004).

[23] N. Rowley and P. Colombani, Phys. Rev. C 11, 648 (1975).

[24] Andreas Gorgen, and Wolfram Korten, J. Phys. G: Nucl. Part. Phys. 43, 024002 (2016).

[25] L.Grodzins, et al, Phys. Letter. 21, 214 (1966).

[26] F. K. McGowan and P. H. Stelson, Phys. Rev. 109, 901 (1958).

[27] W.T. Chou, N. V. Zamfir, and R. F. Casten, Phys. Rev. C 56, 829 (1997).

[28] K. Heyde, P. Van Isacker, M. Waroquier, and J. Moreau, Phys. Rev. C 29, 1420 (1984).

[29] O. Scholten, Phys. Rev. C 28, 1783 (1983).

[30] R. L. Hatch and S. Levit, Phys. Rev. C 25, 614 (1982).

[31] Cheng-Li Wu, et al, Phys. Rev. C 26, 308(R) (1982).

[32] Michael Bender, et al, Phys. Rev. Mod. 75, 121 (2003).

[33] J. W. Negele, Phys. Rev. Mod. 54, 913 (1982).

[34] Michael Bender, et al, Rev. Mod. Phys. 75, 121 (2003).

[35] Balazs Rozsnyai, Phys. Rev. 124, 860 (1961).

[36] Wen Hui Long, et al, Phys. Rev. C 81, 024308 (2010).

[37] T. Niksic, N. Paar, Computer Physics Communications, 185, 18081821 (2014).

[38] J. Ljungvall, et al, Phys. Rev. Lett 100, 102502 (2008).

[39] Yosuke Toh, et al, Journal of nuclear science and technology 497-499 (2002).

[40] J. M. Arias, J. E. Garcia-Ramos, and J. Dukelsky, Phys. Rev. Lett. 93, 212501 (2004).

[41] V. Werner, N. Pietralla, et al, Phys. Rev. C 61, 021301 (2000).

[42] Irving O. Morales, Alejandro Frank, et al, Phys. Rev. C 78, 024303 (2008).

[43] Alejandro Frank, Piet Van Isacker, and Carlos E. Vargas, Phys. Rev. C 69, 034323 (2004).

[44] J. E. Garcia-Ramos and K. Heyde, Phys. Rev. C 92, 034309 (2015).

[45] J. E. Garcia-Ramos and K. Heyde, et al, Phys. Rev. C 89, 034313 (2014).

[46] K. Nomura, R. Rodriguez-Guzman, and L. M. Robledo, Phys. Rev. C 95, 064310 (2017).

[47] K. Nomura, R. Rodríguez-Guzmán, Y. M. Humadi, L. M. Robledo, and H. Abusara, Phys. Rev. C **96** (3), 034310 (2017).

[48] Lu Guo, et al, Phys. Rev. C 76, 034317 (2007).

[49] S. K. Patra, et al, Int. J. Mod. Phys. E 06, 641 (1997).

[50] T. Niksic, et al, Phy. Rev C 65, 054320 (2002).

[51] H. Abusara and Shakeb Ahmad, Phys. Rev. C 96, 064303 (2017).

[52] http://www-phynu.cea.fr/HFB-Gogny_eng.htm

[53] B. D. Serot, J. D. Walecka, Adv. Nucl. Phys. 16 (1986).

[54] R. J. Furnstahl, B. D. Serot, Comments Nucl. Part. Phys. A 2, 23 (2000).

[55] T. Mizutani, F. Myhrer, Phys. Rev. D 35, 1080 (1987).

[56] Y. K. Gambhir, P. Ring, and A. Thimet, ANYALS OF PHYSICS 198, 132-179 (1990).

[57] Y. K. Gambhir, and P. Ring, Modern physiccs Letter A 9, 787-795 (1993).

[58] C. M. Shakin, Wei-Dong Sun, and J. Szweda, Phys. Rev. C 52, 3502 (1995).

[59] Murray Gell-Mann, Phys. Rev. 125, 1067 (1962).

[60] Saul Barshay, Phys. Rev. 108, 1647 (1957).

[61] Y. K. Gambhir, P. Ring, and A. Thimet, ANNALS OF PHYSICS 198, 132-179 (1990).

[62] G. Janssen, K. Holinde, and J. Speth, Phys. Rev. C 49, 2763 (1994).

[63] L. Stodolsky and J. J. Sakurai, Phys. Rev. Lett 11, 90 (1963).

[64] O. Loureno, B. M. Santos, M. Dutra, A. Delfino, Phys. Rev. C 94, 045207 (2016).

[65] O. Lourenco, et al, Phys. Rev. C 80, 045206 (2009).

[66] T. Nik, D. Vretenar, and P. Ring, Phys. Rev. C 78, 034318 (2008).

[67] Satoshi Yoshida, and Hiroyuki Sagawa, Phys. Rev. C 77, 054308 (2008).

[68] J. Bardeen, L. N. Cooper, and J. R. Schrieffer, Phys. Rev. 108, 1175 (1957).

[69] K. L. Kowalski, Phys. Rev. D 2,812 (1970).

[70] P. Moller, et al, arXiv: 1508. 06294 (2015).

[71] Naoki Tajima, Norifumi Suzuki, Phys. Rev. C 64, 037301 (2001).

[72] R. K. Nesbet, Phys. Rev. 109, 1017 (1958).

[73] K. H. Speidel, O. Kenn, and F. Nowacki, Prog. Part. Nucl. Phys 49, 91 (2002).

[74] http://www.nndc.bnl.gov